Degree Project in Vehicle Engineering

Second cycle, 30 credits

Evaluating Aerodynamic Performance and Particle Dynamics in a New Climatic Wind Tunnel using CFD

ANDREA FORTUNATO

Stockholm, Sverige 2025

Evaluating Aerodynamic Performance and Particle Dynamics in a New Climatic Wind Tunnel using CFD

Andrea Fortunato

Master of Science in Engineering
Master Programme in Vehicle Engineering
KTH Royal Institute of Technology

Supervisors at Volvo Cars: Tobias Eidevåg, Anders Karlsson
Supervisor at KTH: Alessandro Talamelli
Examiner at KTH: Mikael Nybacka

Date of presentation: 04/14/2025

TRITA-SCI-GRU 2025:036

KTH Royal Institute of Technology
School of Engineering Sciences
KTH SCI SE-100 44 Stockholm, Sweden
URL: http://www.kth.se/sci

Abstract

Contaminants such as dirt, mud, snow and rain can impair driver visibility and sensor functionality making driving in adverse weather conditions a safety concern. This study focuses on rain contamination of a passenger vehicle in three different wind tunnels at Volvo Cars: an aerodynamic wind tunnel with slotted walls, an old climatic wind tunnel, and a new climatic wind tunnel, both with open jet layouts. The research aims to investigate their airflow and particle transport properties to understand the unique characteristics of each tunnel and their suitability for specific applications.

The investigation is conducted through CFD simulations of the wind tunnels, examining the airflow and particle dynamics in the empty test sections first, and then with a test vehicle. The findings highlight a different sensitivity of each tunnel to boundary interference, such as blockage effects and horizontal buoyancy. The more sensitive a wind tunnel is to such effects, the more the flow field will differ from open road driving and consequently the way the particles are transported.

The results indicate that the aerodynamic wind tunnel closely replicates open road conditions, providing reliable drag measurements and acts as a baseline for soiling pattern. The old climatic wind tunnel shows significant flow acceleration and over-expansion due to its smaller nozzle and the vehicle being very close to it, which makes it too sensitive to blockage effects leading to inaccurate force measurements and peculiar soiling patterns due to the shear layer influence. The new climatic wind tunnel demonstrates a more moderate sensitivity to boundary interference effects, with a wider nozzle and increased distance to the vehicle, offering a balanced approach for both aerodynamic and contamination testing. In summary each wind tunnel provides different vehicle soiling patterns that could be more or less realistic to the driving scenarios of the customers.

This research provides valuable insights into the design and optimization of wind tunnels for automotive testing. It emphasizes the importance of considering boundary interference effects in different wind tunnel layouts and underlines how fundamental it is to clearly outline the specific goals of different tests as their relevance could be questioned. The findings contribute to the development of safer vehicles by proposing multiple testing conditions.

Keywords

Climatic wind tunnel, Aerodynamics, Contamination, Multiphase flows, Computational Fluid Dynamics (CFD) simulations, Open jet, Slotted walls, Exterior water management, Soiling, Adverse weather conditions, Particle dynamics, Turbulence, Transport phenomena, Shear layers

Sammanfattning

Föroreningar som smuts, lera, snö och regn kan försämra förarens sikt och sensorfunktioner, vilket gör körning under ogynnsamma väderförhållanden till ett säkerhetsproblem. Denna studie fokuserar på regnkontamination av ett passagerarfordon i tre olika vindtunnlar hos Volvo Personvagnar: en aerodynamisk vindtunnel med slitsade väggar, en gammal klimatvindtunnel och en ny klimatvindtunnel, båda med öppna jetplanlösningar. Forskningen syftar till att undersöka deras luftflödes- och partikeltransportegenskaper för att förstå varje tunnels unika egenskaper och deras lämplighet för specifika tillämpningar.

Undersökningen genomfördes genom CFD-simuleringar av vindtunnlarna, där luftflödet och partikeldynamiken först undersöktes då testsektionerna var tomma och sedan med ett insatt testfordon. Resultaten visar att varje tunnel är känslig för gränsinterferens, såsom blockeringseffekter och horisontell flytkraft. Ju känsligare en vindtunnel är för sådana effekter, desto mer kommer flödesfältet att skilja sig från körning på öppen väg och följaktligen det sätt på vilket partiklarna transporteras.

Resultaten indikerar att den aerodynamiska vindtunneln nära replikerar öppna vägförhållanden, ger tillförlitliga luftmotståndsmätningar och fungerar som referens för nedsmutsningsmönster. Den gamla klimatvindtunneln uppvisar betydande flödesacceleration och överexpansion på grund av dess mindre munstycke och att fordonet är mycket nära det, vilket gör det för känsligt för blockeringseffekter som leder till felaktiga kraftmätningar och speciella nedsmutsningsmönster på grund av skjuvskiktets påverkan. Den nya klimatvindtunneln uppvisar en mer måttlig känslighet för gränsinterferenseffekter, med ett bredare munstycke och ökat avstånd till fordonet, vilket erbjuder ett balanserat tillvägagångssätt för både aerodynamik- och föroreningstester. Sammanfattningsvis ger varje vindtunnel olika fordonsnedsmutsningsmönster som kan vara mer eller mindre realistiska för kundernas körscenarier.

Denna forskning ger värdefulla insikter om design och optimering av vindtunnlar för fordonstestning. Det understryker vikten av att beakta gränsinterferenseffekter i olika vindtunnellayouter och understryker hur grundläggande det är att tydligt beskriva de specifika målen för olika tester eftersom deras relevans kan ifrågasättas. Resultaten bidrar till utvecklingen av säkrare fordon genom att föreslå flera testförhållanden.

Nyckelord

Klimatvindtunnel, Aerodynamik, Kontaminering, Flerfasflöden, CFD-simuleringar, Öppen jet, Slitsade väggar, Exteriör vattenhantering, Nedsmutsning, Ogynnsamma väderförhållanden, Partikeldynamik, Turbulens, Transportfenomen, Skjuvlager

Acknowledgments

This thesis project has been carried out at Volvo Cars and is the culmination of my academic journey in the Master of Science degree in Vehicle Engineering at KTH Royal Institute of Technology.

First of all, I would like to thank my supervisors at Volvo Cars, Tobias Eidevåg and Anders Karlsson, for their guidance and insight which have been a source of immense growth and inspiration. It has been a privilege to share this important milestone with you. Thank you for always challenging my understanding of things by providing valuable feedback. I am deeply grateful for your encouragement during the difficulties that I encountered.

I would like to extend my heartfelt appreciation to all the colleagues of the Contamination team for their help and support, and for making every day in the office a pleasure to be there.

Special thanks to professors Alessandro Talamelli and Mikael Nybacka, my academic supervisor and examiner, for their expertise and assistance throughout this journey.

Thanks to my closest friends for their constant presence and the vital role they play in my life.

Finally, my deepest gratitude goes to my parents, my brother and my girlfriend for always being there for me and being my number one supporters.

Gothenburg, March 2025
Andrea Fortunato

"For every fact there is an infinity of hypotheses."

– Robert M. Pirsig,
Zen and the Art of Motorcycle Maintenance: An Inquiry into Values

Contents

List of Figures

List of Tables

List of acronyms and abbreviations

AWT	Aerodynamic Wind Tunnel
CFD	Computational Fluid Dynamics
CFL	Courant-Friedrichs-Lewy
CWT	Climatic Wind Tunnel
CWT1	Old Climatic Wind Tunnel
CWT2	New Climatic Wind Tunnel
DES	Detached Eddy Simulation
DNS	Direct Numerical Simulation
LES	Large Eddy Simulation
RANS	Reynold Averaged Navier-Stokes

List of Symbols Used

$\boldsymbol{\omega}$	Fluid vorticity, see equation (2.15),	page 11
Δt	Computational timestep, see equation (2.3),	page 7
η	Kolmogorov lenght scale, see equation (2.2),	page 6
λ	Taylor length scale, see equation (2.6),	page 8
$\mathbf{U_s}$	Particle slip velocity, see equation (2.7),	page 9
∇P_f	Pressure gradient of the fluid, see equation (2.11),	page 10
ρ_f	Fluid density, see equation (2.1),	page 6
ρ_p	Particle density, see equation (2.8),	page 9
τ_f	Characteristic time of the flow, see equation (2.9),	page 9
τ_p	Particle relaxation time, see equation (2.8),	page 9
A_p	Particle cross-sectional area, see equation (2.12),	page 10
C_D	Drag coefficient, see equation (2.12),	page 10
C_p	Static pressure coefficient, see equation (5.1),	page 29
$C_{D,sphere}$	Spherical drag coefficient, see equation (2.13),	page 10
C_{LS}	Shear lift coefficient, see equation (2.15),	page 11
D_p	Particle diameter, see equation (2.7),	page 9
F_P	Pressure gradient force, see equation (2.11),	page 10
L	Integral length scale, see equation (2.2),	page 6
m_p	Particle mass, see equation (2.10),	page 10

N_t Nodes of the temporal grid, see equation (2.4), ... page 7

P_s Static pressure, see equation (5.1), ... page 29

$P_{s,c}$ Static pressure in the calibration point, see equation (5.1), . . . page 29

Re Reynolds number, see equation (2.1), ... page 6

Re_p Particle Reynolds number, see equation (2.7), ... page 9

Re_s Shear flow Reynolds number, see equation (2.16), ... page 11

St Stokes number, see equation (2.9), ... page 9

U Integral velocity, see equation (2.3), ... page 7

U_c Velocity in the calibration point, see equation (5.1), ... page 29

V_p Particle volume, see equation (2.11), ... page 10

y Distortion interpolation parameter, see equation (2.14), ... page 10

Chapter 1

Introduction

In recent years, the impact of adverse weather conditions on transportation has become a critical research field. According to Eisenberg et al. [1], the first snowfall of the season significantly increases the fatality rate of car accidents. Therefore, it is important to study vehicle interaction with external agents as it can impair driver and camera visibility and limit sensor functionality due to rain, snow, or dirt obstruction. Such phenomena are referred to as surface contamination; in particular, when the surface contaminant is water, it is called soiling or exterior water management [2].

The way a vehicle is contaminated is a consequence of the airflow around it, thus soiling patterns can be manipulated with the aerodynamic shape of the vehicle. By controlling the contamination, it is possible to reduce maintenance costs, extend the lifespan of exposed components and improve fuel efficiency by maintaining predictable aerodynamic performance, even under solid contaminants deposits that might otherwise alter the shape of the vehicle.

Apart from test driving the car in the desired weather conditions, the tools to study aerodynamics and vehicle contamination are wind tunnel experiments and Computational Fluid Dynamics (CFD). These methods complement each other, with wind tunnels providing experimental validation for CFD models. The constantly evolving computing power makes CFD an affordable, sustainable and time-efficient alternative, but its models always need proper validation against experimental data such as wind tunnel testing. Both methods make it possible to perform season-independent testing, eliminating the need to wait for suitable climatic conditions to run specific tests.

1.1 Objectives and Limitations

Volvo Cars has recently constructed a new Climatic Wind Tunnel (CWT) which complements their existing aerodynamic and older climatic wind tunnels. This results in a total of three wind tunnels, one aerodynamic and two climatic.

1.1.1 Purpose

The purpose of this work is to investigate and compare, through CFD simulations, the differences between three different wind tunnels, each having unique dimensions, layouts and devices that significantly affect their aerodynamics and particle transport properties. It is driven by the interest in understanding the characteristics of the new climatic wind tunnel at Volvo Cars and determining the suitability of each wind tunnel for specific applications. Then, a turbulence generator will be simulated in the new climatic wind tunnel as an attempt to replicate the more turbulent flow of real world driving and its influence on the exterior soiling of the vehicle.

1.1.2 Research Methodology

The evaluation of aerodynamic performance and particle dynamics in wind tunnels will be conducted through CFD simulations by examining both the airflow in the empty test sections and the interaction between the test object and the tunnels. The particle dynamics will be evaluated after that, as it is strongly dependent on the airflow. The contaminant injected is water to simulate a rainfall scenario. Three different sizes of raindrops will be injected in front of the car from injection points in the wind tunnel nozzles.

The airflow will be compared by means of pressure gradients in the empty tunnels and boundary interference. Thereafter, drag, skin friction coefficient and rain mass accumulated on the car will be analyzed.

1.1.3 Goals

The project is divided into the following steps:

1. Evaluate the airflow difference in the three wind tunnels.
2. Compare the exterior soiling of the car in the three tunnels.

3. Investigate the influence of a turbulence generator in the new climatic wind tunnel from a contamination perspective.

1.1.4 Limitations

Given the scope of this work, it is fundamental to consider the limitations that might impact the general validity of the results. The main limitation in the field of engineering simulations is validating the method against experimental results. It was decided that the entirety of this research would lie on numerical simulations due to time restrictions and the availability of the new climatic wind tunnel which has been constructed but it is not yet fully operational. Thus, the attempt to validate the simulations relies fully on the literature. However, the available literature only provides data about the Volvo Cars aerodynamic wind tunnel and lacks data on the two climatic ones.

Furthermore, the level of detail in the geometry of the tunnels is essential for the accuracy of the results. The complete geometries of the AWT and new CWT are sufficiently detailed representations of reality, meanwhile, the old CWT lacks the contraction geometry, so its inlet was modeled as a straight nozzle matching the length of its real counterpart to account for flow development. Then, due to complexity, all the wind tunnels do not include the complete loop and their flow conditioning devices have not been implemented or disabled where available. This applies for all tangential blowers, wheel drive units and moving floors except for the suction scoop, which is kept active in the AWT.

Another detail to consider is the stick boundary condition for the rain droplets. This approach was chosen to better track the contaminated areas of the car in the tunnels, but in reality droplets slide on the surface because of the wall shear stress. In fact, wall shear stress is expected to vary between tunnels, altering the water film formation on the vehicle.

Finally, the chosen injectors grid may not be optimal for all wind tunnels and not realistic for the open-road simulation, but its concept aims at amplifying the difference between the simulated scenarios.

1.2 Outline

The next chapter explains the theoretical context in fluid mechanics and multiphase flows. Then, Chapter 3 presents the general theory of automotive wind tunnels with focus on boundary interference followed by the detailed description of the three Volvo Cars wind tunnels. Chapter 4 presents the

methodological approach taken towards the setup of the simulations. The results are discussed in Chapter 5, followed by the conclusions and possible approaches to continue this type of investigation.

Chapter 2

Background

2.1 Computational Fluid Dynamics

Computational Fluid Dynamics (CFD) is a subfield of fluid mechanics focused on modeling continuous domains through spatial and time discretization. The mathematical models applied require careful validation to provide reliable insights about the flow phenomena simulated.

In multiphase CFD simulations, the accuracy of the model is crucial to obtain the correct airflow and predict realistic particle trajectories. The multiphase models are coupled to the airflow properties, therefore, an inaccurate airflow will deliver unreliable particle dynamics. This makes accuracy the main concern when interpreting CFD simulations.

Previous studies have performed validation of CFD simulations of wind tunnels. For instance, Ljungskog's [3] research investigates the properties of a slotted walls wind tunnel and aims to enhance the accuracy of its virtual counterpart by providing validation between simulations and physical measurements. Similarly, Zhang et al. [4] addresses the consistency between the natural rainfall scenario and the one replicated in a virtual climatic wind tunnel. The authors validated both airflow and vehicle soiling in the simulations against physical wind tunnel experiments.

2.2 Turbulence

Turbulence is a complex and chaotic phenomenon that occurs in fluid flows, characterized by irregular fluctuations and vortex structures called eddies. It is caused by disturbances in the flow whose inertia overcomes viscous damping. The ratio of flow inertia over viscous forces is depicted by the non-dimensional

Reynolds number, named after Osborne Reynolds:

$$Re = \frac{\rho_f U L}{\mu_f} \tag{2.1}$$

where ρ_f is the fluid density, U is the characteristic velocity, L is the characteristic or integral length scale of the flow and μ_f is the dynamic viscosity of the fluid [5]. For instance, when considering $U = 70$ km/h and the length of the car as $L = 4.26$ m, the Reynold number results in $Re = 6 \cdot 10^6$.

Turbulent eddies dissipate kinetic energy in the so called energy cascade. Smaller eddies receive energy from the larger ones with no dissipation until the turbulent structure is small enough to be dominated by viscosity, rather than inertia.

Consequently, the turbulent structures are necessary smaller than the intergral length scale L of the domain and larger than the Kolmogorov [6] length scale η, where viscosity is dominant and kinetic energy is dissipated.

The ratio between Kolmogorov and the integral length scales is estimated to be proportional to the Reynolds number [7]:

$$\frac{\eta}{L} \approx Re^{-3/4} \tag{2.2}$$

Accurately modeling turbulence in CFD is still an engineering challenge and several numerical methods have been developed. This section provides an overview of the most relevant ones.

2.2.1 Direct Numerical Simulation

The Direct Numerical Simulation (DNS) method discretizes the Navier-Stokes equations and solves turbulence without modeling it. However, DNS methods are not feasible in industrial applications due to their computational cost. Completely solving turbulence requires the smallest spatial and temporal scales.

The spatial scale is the Kolmogorov microscale. The inverse of Equation 2.2 represents the number of nodes in one dimension, thus proportional to $Re^{3/4}$. Consequently, for a generic three dimensional flow, the spatial grid would be proportional to $(Re^{3/4})^3 = Re^{9/4}$.

The temporal scale is given by the Courant-Friedrichs-Lewy (CFL)

condition [8] for numerical stability:

$$\frac{U\Delta t}{\eta} < 1 \tag{2.3}$$

where Δt is the temporal microscale, or timestep. Equation 2.3 is the condition for which the timestep is sufficiently short so that a flow particle does not travel more than the spatial microscale η in the said timestep. Considering a simulated time of the same order of magnitude of the integral time scale $T = L/U$, the nodes of the temporal grid would be $N_t = T/\Delta t$. After applying Equation 2.2 and 2.3:

$$N_t = \frac{T}{\Delta t} = \frac{L}{U\Delta t} > \frac{LU}{U\eta} = \frac{L}{\eta} \approx Re^{3/4} \tag{2.4}$$

Combining spatial and temporal grids, the total number of nodes to completely solve the turbulent Navier-Stokes equations is proportional to $Re^{9/4} \cdot Re^{3/4} = Re^3$. This proves how unfeasible the DNS method is, especially for high Reynolds flows.

2.2.2 Reynolds Averaged Navier-Stokes

The Reynolds Averaged Navier-Stokes (RANS) equations consist in solving the mean flow directly and modeling all fluctuations according to the Reynolds decomposition through additional terms known as Reynolds stresses. The Reynolds decomposition in time is expressed as follows:

$$x = \langle x \rangle + x' \tag{2.5}$$

where x is a quantity of interest, $\langle x \rangle$ is its time-averaged component and x' is its time-fluctuating component.

RANS models are popular because of their relatively low computational cost. There is no constraint on the required length scale: it has to be relatively small merely to guarantee numerical stability and sufficient accuracy of the flow field. However, this approach models all the turbulence so it might be an excessive approximation of reality, especially when trying to model large turbulent structures that are the most affected by boundary conditions.

2.2.3 Large Eddy Simulation

The idea behind the Large Eddy Simulation (LES) method comes from Smagorinsky's [9] intuition of finding a compromise between DNS and RANS. The goal is to solve only big-scale turbulent eddies that are affected by boundary conditions and model the smaller ones. To do this, an intermediate scale between the integral and Kolmogorov's has to be defined. It is called Taylor microscale λ and its purpose is to distinguish large turbulent eddies dominated by inertia from small eddies dominated by viscosity. Just as the Kolmogorov's, also the Taylor microscale can be related to the Reynolds number through the ratio with the integral scale [10] resulting in:

$$\frac{\lambda}{L} = Re^{-1/2} \tag{2.6}$$

This results in a significant reduction in the computational cost compared to DNS methods.

2.2.4 Detached Eddy Simulation

Despite the computational time improvement of LES compared to DNS, LES still requires excessive mesh refinements in near wall regions resulting again in being unfeasible for industrial applications. Consequently, LES-RANS hybrid methods have been developed like the Detached Eddy Simulation (DES). This results in modeling attached eddies near solid boundaries with the RANS method, while detached eddies in separation areas are modeled according to the LES approach [11]. This makes the DES turbulence model very versatile, efficient and accurate for a wide range of turbulent flows, including those with strong flow separation and complex geometries.

2.3 Multiphase Flows

In fluid dynamics there are two frameworks to describe a flow, the Eulerian and the Lagrangian.

The Eulerian approach consists in a stationary observation of the airflow at fixed locations, meanwhile the Lagrangian focuses on individual particles as they move in a flow field. In the context of multiphase flows, both frameworks are fundamental to study the flow properties and particle dynamics.

In multiphase flows, the distinct phases are coupled which means that there is an interaction between each other. The particles are subject to the motion

of flow field and the presence of particles in a fluid will alter its airflow. When this mutual effect is non-negligible, the flow is considered two-way coupled. However, when the particles are small enough that they do not affect the surrounding flow field, it is called one-way coupled.

2.3.1 Particle Dynamics

Given that the airflow in a wind tunnel is generally turbulent, it is important to describe particle dynamics in such environment to understand transport phenomena and interaction with the flow. Particle transport can be quantified by means of dimensionless numbers. The particle Reynolds number classifies the surrounding flow based on the local turbulence:

$$Re_p = \frac{\rho_f \, D_p \, |\mathbf{U_s}|}{\mu_f} \tag{2.7}$$

where $\mathbf{U_s}$ is the particle slip velocity and D_p is the particle diameter. When $Re_p < 1$ the local flow is dominated by viscosity and it is called Stokes flow.

A measure of how quickly a particle responds to fluctuations in the flow field is the particle relaxation time τ_p. It generally has an integral form for $Re_p > 1$ but for a Stokes flow it can be derived as:

$$\tau_p = \frac{\rho_p D_p^2}{18 \mu_f} \tag{2.8}$$

From the particle relaxation time the dimensionless Stokes number can be derived:

$$St = \frac{\tau_p}{\tau_f} \tag{2.9}$$

where τ_f is the characteristic time of the fluid flow. The Stokes number, strongly dependent on the particle relaxation time, clearly quantifies how the particle follows the fluctuations in the flow field.

- For $St << 1$ the particle rapidly adjusts to changes in the flow
- For $St >> 1$ the particle's inertia prevails and it might not follow the flow

2.3.1.1 Droplet Equation of Motion

This thesis will focus on rain droplets, therefore, the particles described here are liquid. The general equation of motion for a particle is given by Newton's

second law:

$$\sum_i F_i = m_p \frac{d^2 |\mathbf{U_p}|}{dt^2} \tag{2.10}$$

where $|\mathbf{U_p}|$ is the particle velocity and m_p is the particle mass. The left hand side in Equation 2.10 is the sum of all surface and volume forces acting on a particle. They are gravity, pressure gradient, collisions between particles, drag and lift forces.

When a pressure gradient is present in the flow, the particle will be subject to its force:

$$\mathbf{F_P} = -V_p \nabla P_f \tag{2.11}$$

where V_p is the particle volume and ∇P_f is the pressure gradient of the fluid.

The drag force acting on a particle originates from its slip velocity relative to the flow and is generally formulated as follows:

$$\mathbf{F_D} = \frac{1}{2} \rho_f C_D A_p |\mathbf{U_s}| \mathbf{U_s} \tag{2.12}$$

where C_D is the drag coefficient, where A_p is the particle cross-sectional area. The drag coefficient is not constant and it has been shown to depend on the particle Reynolds number and its shape. The Schiller-Naumann correlation [12] for spherical particles computes C_D for different Re_p regimes:

$$C_{D,sphere} = \begin{cases} \frac{24}{Re_p} \left(1 + 0.15 Re_p^{0.687}\right) & \text{for } Re_p < 1000 \\ 0.44 & \text{for } Re_p \geq 1000 \end{cases} \tag{2.13}$$

However, under the influence of aerodynamic forces, a liquid droplet is deformed. This requires a model to account for it such as the Liu's correlation, which applies an interpolation between the drag coefficients of spherical and distorted disc-shaped droplets:

$$C_D = (1 + 2.632y) C_{D,sphere} \tag{2.14}$$

where $y \in (0, 1)$ is the distortion interpolation parameter.

The shear lift force acting on particles is generated by velocity gradients in orthogonal directions to the flow and is defined as:

$$F_{LS} = C_{LS} \frac{\pi}{8} \rho_f D_p^3 (\mathbf{U_s} \times \boldsymbol{\omega}) \tag{2.15}$$

where C_{LS} is the shear lift coefficient and ω is the fluid vorticity. C_{LS} can be computed with the Sommerfeld [13] correlation method where C_{LS} is a function of Re_p and the shear flow Reynolds number Re_s defined as:

$$Re_s = \frac{\rho_f D_p^2 \left|\omega\right|}{\mu_f} \tag{2.16}$$

Now C_{LS} can be computed as:

$$C_{LS} = \frac{4.1126}{Re_s^{0.5}} f(Re_p, Re_s) \tag{2.17}$$

with the correction function:

$$f(Re_p, Re_s) = \begin{cases} (1 - 0.3314\beta^{0.5})e^{-0.1Re_p} + 0.3314\beta^{0.5} & \text{for } Re_p \leq 40 \\ 0.0524(\beta Re_p)^{0.5} & \text{for } Re_p > 40 \end{cases} \tag{2.18}$$

and with:

$$\beta = 0.5\frac{Re_s}{Re_p} \tag{2.19}$$

For further information on the droplet equation of motion and droplet integrity, please refer to Hamidi [14].

Chapter 3

Automotive Wind Tunnels

The purpose of automotive wind tunnels is to replicate the condition of driving a car through still air on a flat road. However, the wall boundaries of a wind tunnel over-constrain the airflow compared to an open road, which would otherwise be influenced only by the floor. This phenomenon is called boundary interference [3] and is divided into different categories of effects [15].

3.1 Boundary Interference Effects

The most relevant boundary interference effects for this thesis are described here. Each of them has been studied in depth, leading to the derivation of correction methods. However, in this work, the correction methods were deliberately neglected in order to compare raw data and emphasize the differences between the wind tunnels.

3.1.1 Nozzle Blockage

The presence of the vehicle in the test section is also perceived upstream inside the nozzle with airflow displacement that will experience further blockage from the walls. The consequence is a faster air speed at the nozzle compared to the empty tunnel.

3.1.2 Solid Blockage

The solid blockage effect, as the name suggests, is due to the presence of a physical blockage in the test section. In a closed wall test section, the available

cross-sectional area for the fluid to flow through is reduced and the streamlines cannot expand as they would in a natural scenario due to the presence of the wind tunnel boundaries. Consequently, the airflow accelerates around the vehicle to preserve continuity, increasing the measured drag.

The opposite happens in an open jet test section. There is airflow deceleration due to its over-expansion around the vehicle reducing the measured drag. Moreover, this phenomenon is amplified the more the test object approaches the nozzle. Its proximity increases the flow angle, which results in a further jet expansion and separation from the test object.

Both the nozzle and solid blockage can be visualized by means of velocity magnitude in Figure 3.1

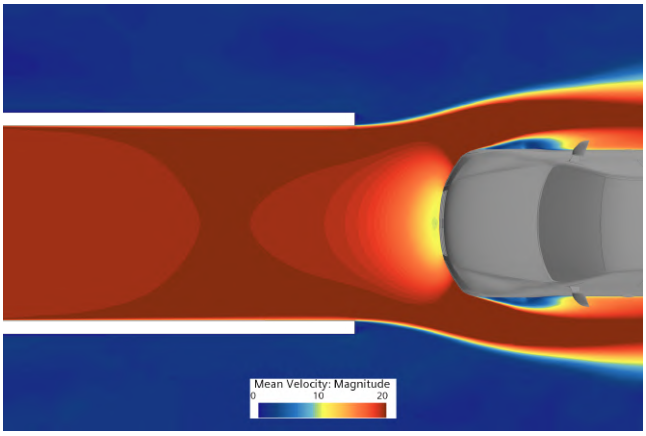

Figure 3.1: Nozzle and solid blockage effects in an open jet wind tunnel.

3.1.3 Pressure Gradient and Horizontal Buoyancy

The longitudinal pressure gradient in the empty test section strongly affects the quality of the measurements as it causes horizontal buoyancy. Horizontal buoyancy for closed walls wind tunnels can be understood with pipe flow analogy. The boundary layer build-up on the walls will cause the flow to accelerate to maintain continuity. According to Bernoulli's conservation principle, the pressure will decrease in the streamwise direction. This favorable pressure gradient leads to increased drag measurements due to the buoyancy effect generated by a higher pressure in front of the car and a lower pressure in the rear.

In open jet wind tunnels, the pressure drops when exiting the nozzle and should stay constant until the flow decelerates to enter the collector, causing the pressure to rise again. When compared with closed walls wind tunnels,

open jet configurations experience significantly larger pressure gradients.

3.2 Self-Correcting Wind Tunnels

The boundary interference effects just described can vary significantly not only between different wind tunnel layouts, but also within the same test section due to vehicle positioning. This suggests the possibility of developing wind tunnels that are ”self-correcting” in a way that the boundary interference effects can balance each other [3] by reducing the dependency on the test object and minimizing the errors.

3.2.1 Slotted Walls

The concept of slotted walls stems from the need to reduce the blockage effect and allow expansion of the flow into longitudinal openings in the test section walls, called slots. The benefits of this layout consists in being an hybrid approach between open and closed configurations. Allowing airflow expansion while maintaining a long usable test section of closed wall wind tunnels by avoiding shear layer instabilities of an open jet. Although this approach brings tangible benefits to the reduction of boundary interference, correction methods for slotted walls wind tunnels are necessary and based on the closed wall layout.

3.2.2 Open Jet

In self-correcting open jet wind tunnels, the flow is free to expand around the vehicle in the test chamber. Balancing the blockage from the nozzle and flow over-expansion requires optimization of the distance of the car from the nozzle. Mercker and Wiedermann [16] proposed new correction methods in 1996 and Wickern [17] established the theoretical foundations for designing self-correcting open jet wind tunnels. The main key findings resulted in a proper tuning in the distance between the nozzle exit and the test object and establishing an optimal test section length to eliminate interference caused by the collector. Furthermore, Wickern [17] suggests that when the test object is moved closer to the nozzle, the open jet tends to behave in a way that is comparable to slotted walls layout.

3.3 Volvo Cars Wind Tunnels

Volvo Cars wind tunnels belong either to the slotted walls or to the open jet categories. This section describes the three tunnels and highlights their differences.

3.3.1 Aerodynamic Wind Tunnel

The Volvo Cars Aerodynamic Wind Tunnel (AWT), also know as PVT, was originally built in 1986. It is a closed return, horizontal loop type with slotted wall test section. It was later upgraded in 2006 to the current specifications [18], including a five belt moving ground system and a 5 MW fan which allows to test wind speeds up to 250 km/h. It is equipped with a suction scoop for boundary layer removal before the test section and distributed suction. The car is placed on a turntable that allows testing different yaw angles. Moreover, it is possible to use a rain grid to inject droplets to test rainfall scenario. Together with devices to control humidity and temperature, it is a multipurpose tunnel for aerodynamic, climatic and thermodynamic testing. However, for contamination purposes, it is possible to inject only rain, not snow. An overview of the technical specifications of the AWT is provided in Table 3.1 and its geometry in Figure 3.2.

Table 3.1: Technical specifications of the Aerodynamic Wind Tunnel. [3]

Type	Slotted Walls
Nozzle to front wheel	4.1 m
Contaminants	Only rain, no snow
Temperature range	20 °C to 60 °C
Flow conditioning devices	Suction scoop, distributed suction and aft-belt tangential blowing

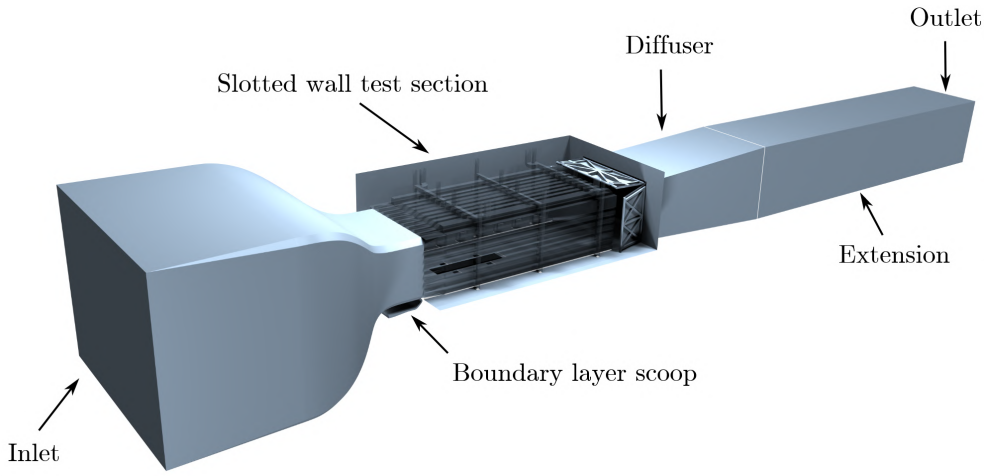

Figure 3.2: Geometry of the Aerodynamic Wind Tunnel [3].

3.3.2 Old Climatic Wind Tunnel

The Old Climatic Wind Tunnel (CWT1) was constructed in 1972 and underwent major upgrades over the years. It is an open jet type with closed, horizontal loop and allows wind speeds up to 200 km/h. It is equipped with systems to control humidity and temperature and both rain and snow can be injected for climatic tests. An overview of its technical specifications is shown in Table 3.2 and its geometry in Figure 3.3.

Table 3.2: Technical specifications of the Old Climatic Wind Tunnel.

Type	Open jet
Nozzle to front wheel	1.85 m
Contaminants	Rain and snow
Temperature range	-40 °C to 50 °C

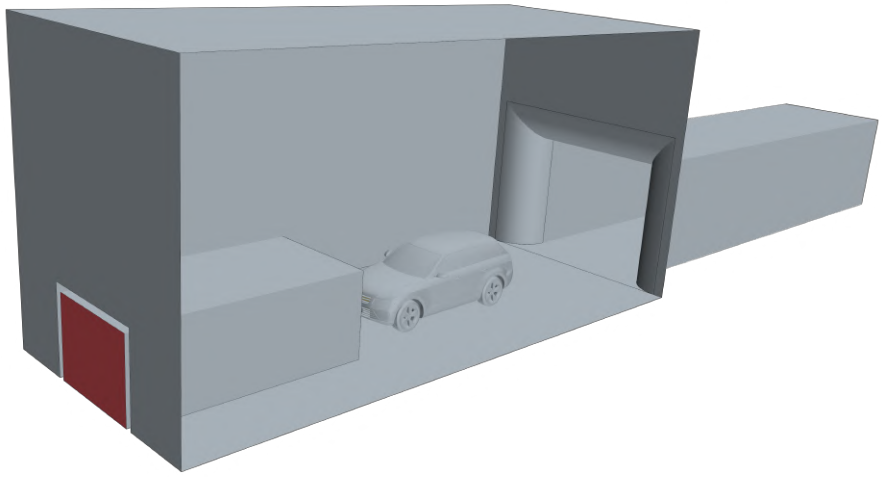

Figure 3.3: Geometry of the Old Climatic Wind Tunnel.

3.3.3 New Climatic Wind Tunnel

The New Climatic Wind Tunnel (CWT2) was built in 2022. The main differences with the CWT1 are a bigger nozzle, a wider test section and the presence of a collector before the diffuser. Both are closed return and open jet, but the flow in the CWT2 follows a vertical loop. Its technical specifications are listed in Table 3.3.

Table 3.3: Technical specifications of the New Climatic Wind Tunnel.

Type	Open jet
Nozzle to front wheels	2.5 m
Contaminants	Rain and snow
Temperature range	-40 °C to 50 °C

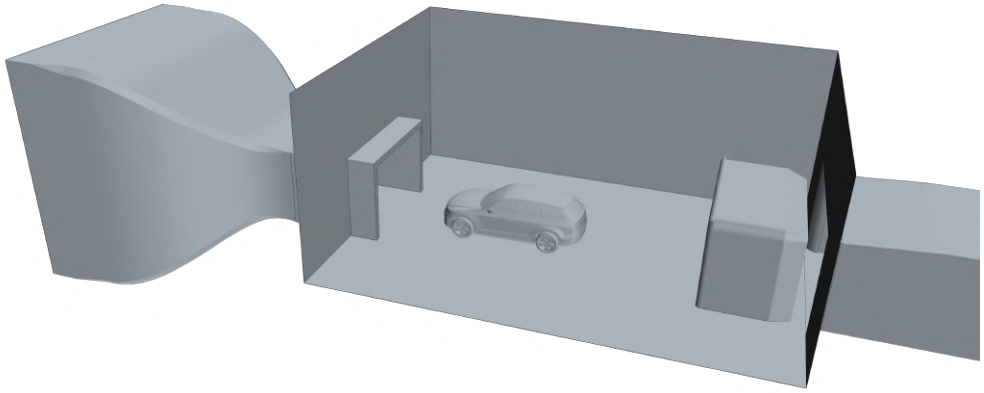

Figure 3.4: Geometry of the New Climatic Wind Tunnel.

3.3.4 Summary and Comparisons

The three wind tunnels described have unique characteristics that make their airflow and particle transport properties differ significantly. First, the layout and boundary interference effects perceived in the tunnels vary between slotted walls and open jet layouts. Table 3.4 provides a clear overview of these differences.

Furthermore, a very distinctive behavior is expected between CWT1 and CWT2 due to their nozzle, test section and vehicle proximity to the nozzle, causing unique boundary interference effects.

Table 3.4: Specification comparison between the three wind tunnels.

	AWT	**CWT1**	**CWT2**
Type	Slotted walls	Open jet	Open jet
Nozzle to front wheels	4.1 m	1.85 m	2.5 m
Contaminants	Rain	Rain and snow	Rain and snow

The wide difference in nozzle sizes is shown in Figure 3.5.

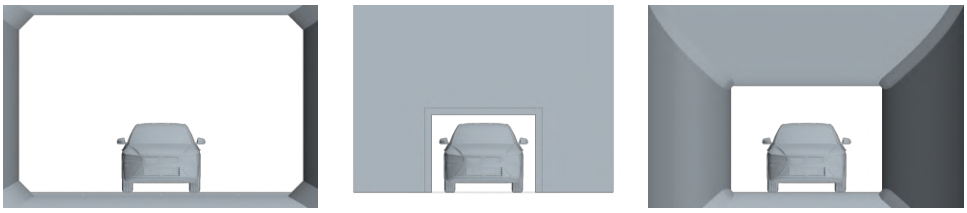

(a) Aerodynamic Wind Tunnel

(b) Old Climatic Wind Tunnel

(c) New Climatic Wind Tunnel

Figure 3.5: Wind tunnels nozzles differences.

Chapter 4

Methodology

4.1 Computational Setup

This section describes the complete simulation workflow. This includes the geometry creation, the boundary and initial conditions, the modeling approach towards the Lagrangian framework, the mesh and solver settings. The simulations were all performed in StarCCM+ 2021.2 by implementing Java macros that would automate the setup process by importing the wind tunnels geometries, placing them in the correct position relative to the car, applying boundary conditions and mesh settings to the domain. This significantly improved the workflow, making it easier to run numerous simulations by removing human error in the setup of each case.

4.1.1 Geometries

First, the CAD models for each wind tunnel and each configuration are necessary. Volvo Cars provided the complete geometry for the aerodynamic wind tunnel and only the contraction for the new climatic wind tunnel. Starting from the CAD geometry of the contraction, the rest of the tunnel was modeled after it was measured. Due to the unavailability of any model for the old climatic wind tunnel, it was created anew after physically measuring it on site and modeling it in a CAD environment. The main issue with the old climatic wind tunnel model is the lack of its contraction, which led to the use of a straight nozzle as an alternative. The length of the straight nozzle matches the length of the physical tunnel nozzle to achieve an accurate boundary layer development. An extension of three diffuser lengths is added between all diffusers and outlet sections. See Figures 3.2, 3.3 and 3.4 for reference.

The chosen test vehicle is the AeroSUV DrivAer model [19]. It consists of a generic SUV geometry whose level of detail is comparable to today's production cars, including an engine bay flow [20]. However, a flat underbody was preferred, instead of a detailed one. This simplifies the computational grid and reduces the cell count. The geometry of the AeroSUV is presented in Figure 4.1

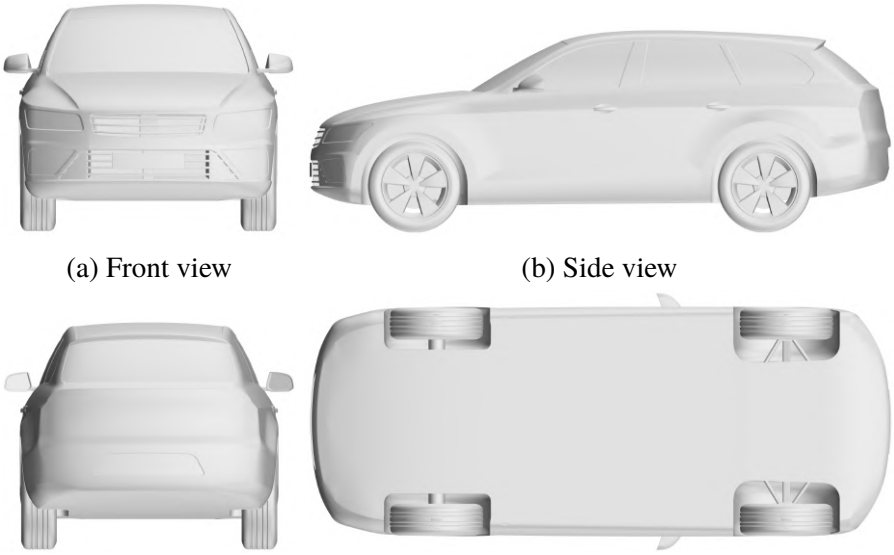

(a) Front view (b) Side view

(c) Rear view (d) Bottom view

Figure 4.1: Views of the AeroSUV geometry.

4.1.2 Boundary and Initial Conditions

The desired airflow velocity is 70 km/h as it is considered more relevant for contamination analysis than the higher magnitudes preferred in aerodynamic testing. It is set as a velocity inlet boundary conditions for all the cases with a straight nozzle. For tunnels with a contraction it was iteratively tuned until the velocity at the calibration points was 70 km/h with a margin of error of ± 1 km/h. Such points correspond to the wind speed calibration coordinates in the physical wind tunnels.

All walls are set as no-slip walls. The outlet section is set to a zero gauge pressure outlet condition.

Although the WDUs are not modeled in the wind tunnel geometries, the wheels are set to rotate.

The fluid phase model is turbulent, incompressible air at 20° C temperature.

4.1.3 Droplet Phase Models

The Lagrangian phases implemented consist of spherical liquid water droplets, one-way coupled, one particle per parcel and with the stick condition on the car surface. Three different phases are injected according to the relevant particle sizes measured when driving behind a truck [21]. The diameters are 5 µm, 50 µm, 200 µm and are kept constant so that each phase is significantly different from the other. This helps to clearly distinguish the behavior of each phase. The respective particle relaxation times are listed in Table 4.1.

Table 4.1: Particle relaxation time of droplet phases.

Particle Diameter D	**Relaxation Time** τ_p
5 µm	$1.56 \cdot 10^{-6} s$
50 µm	$1.56 \cdot 10^{-4} s$
200 µm	$2.49 \cdot 10^{-3} s$

The injection points form a 100 by 75 grid that injects 7500 droplets per phase at each time step. The points are distributed in a rectangle area of 2.3 by 1.7 meters as it is designed to fill up the smallest nozzle of the three tunnels, i.e. CWT1 and is positioned 0.5 m into the nozzle. The same grid is used for all tunnels to highlight the differences among them. Figure 4.2 presents the grid in front of the car inside the nozzle of CWT1.

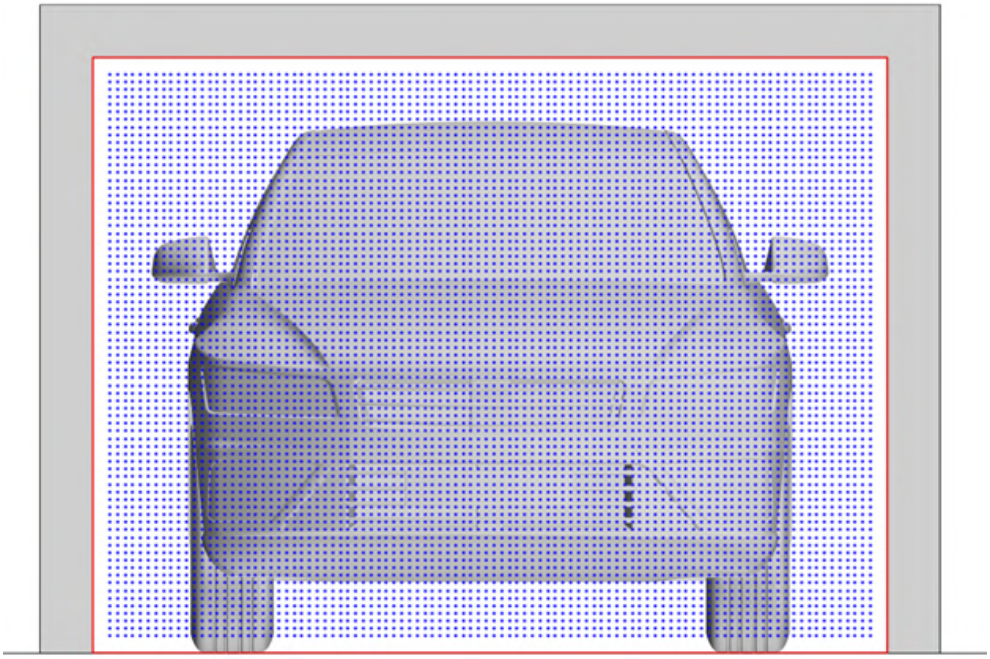

Figure 4.2: Particle injection grid in the nozzle of CWT1. The same grid is used for all tunnels.

4.1.4 Computational Grid

The same meshing approach has been taken for all the wind tunnels and open road domains. The domains are meshed using trimmed hexahedral cells. The all-y^+ treatment is used for the walls. Based on the type of walls the number of prism layers can vary from 1 to 14 with adequate near-wall thicknesses to aim for $y^+ > 30$ on the tunnel walls and $y^+ < 1$ on the car surface. Refinement boxes are in place to adjust the elements size to the appropriate dimension in the desired areas of the domain. The growth rate from one box to the other consists in doubling the element size. Further refinements take place in the nozzle wake. This is necessary to better capture the shear layers in the open jet wind tunnels and when simulating the car. The cell count will then vary significantly based on the tunnel geometry, layout and dimension. The resulting cell counts for the complete tunnels are listed in Table 4.2, while Figure 4.3 shows the computational grids in the cut views of the symmetry planes.

Table 4.2: Mesh cell count for the Volvo Cars wind tunnels.

Wind Tunnel	Empty	Car
AWT	65 M	150 M
CWT1	13 M	104 M
CWT2	25 M	118 M

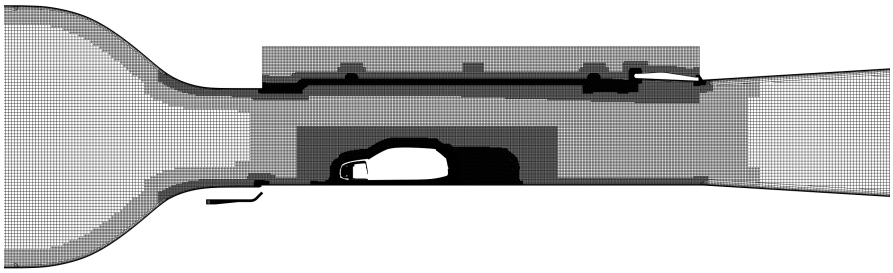

(a) Mesh of the Aerodynamic Wind Tunnel

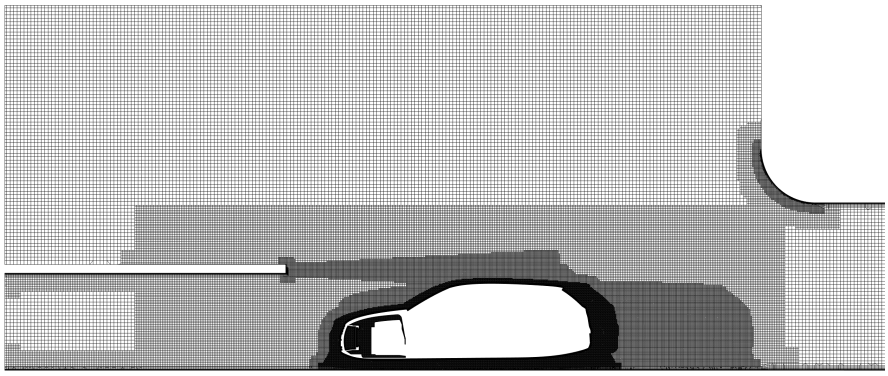

(b) Mesh of the Old Climatic Wind Tunnel

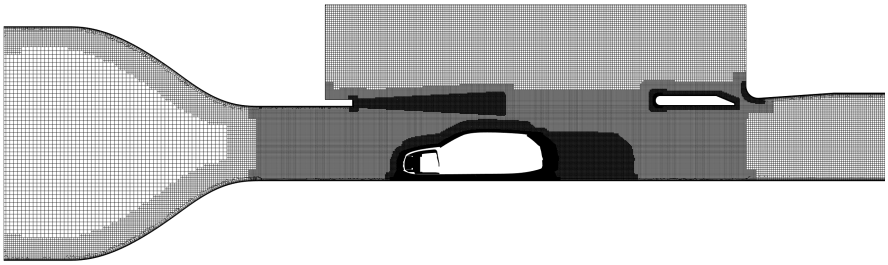

(c) Mesh of the New Climatic Wind Tunnel

Figure 4.3: Cut views of the symmetry planes showing the meshes of the three wind tunnels.

4.1.5 Solver Settings

The physical time simulated is 6.3 s in unsteady state for empty tunnels. Meanwhile, when simulating a car in the tunnels, it was necessary to make sure that the same amount of rain would pass the car. Therefore, once the end time was reached, the injectors were deactivated and the simulations continued for an additional 1.5 s. This way of ”flushing” the wind tunnels is a fundamental step for the comparability of the results due to the different positions of each car in the tunnels, hence different distances from the injectors. If this approach had not been taken the closer the car to the injectors, the more it would be contaminated.

The turbulence model used is DES and the CFL number for the particles is set within the range of 0.05 to 0.35, making the time steps sufficiently short so that all particles would not travel more than one cell per time step.

4.2 Aerodynamics and Soiling Evaluation

The approach to evaluate the airflow in the three wind tunnels starts by assessing the boundary interference effects in the different tunnels. The goal is to establish how much the flow is altered compared to an open road simulation. Each wind tunnel has its own sensitivity to boundary interference and this will result in different forces distribution on the car like drag, pressure and skin friction. On top of that, the transport of droplets will vary significantly. The exterior soiling of the car is compared both visually and by plotting the cumulative amount of rain that impacted the vehicle.

Chapter 5

Results and Discussion

This chapter presents the validation performed on the AWT simulation and the results for the comparison of the three wind tunnels.

5.1 Validation

Before diving into the results, the validation will be briefly discussed in this section. As mentioned in Chapter 1.1.4, no experimental wind tunnel testing has been performed during this project, so validation of the method is merely possible by comparing the results with previous literature. The only Volvo Cars wind tunnel that has been studied and published in depth is the AWT. However, a comparison is meaningful when the same conditions are applied. In this case, the AWT has been simulated in its scoop-only mode where only the suction scoop is activated and the other flow conditioning devices are turned off. A publication that has done the same is the one conducted by Ljungskog [3], who has tested the scoop-only mode for the AWT, but at different velocities. Figure 5.1 presents the longitudinal pressure gradient in the empty AWT.

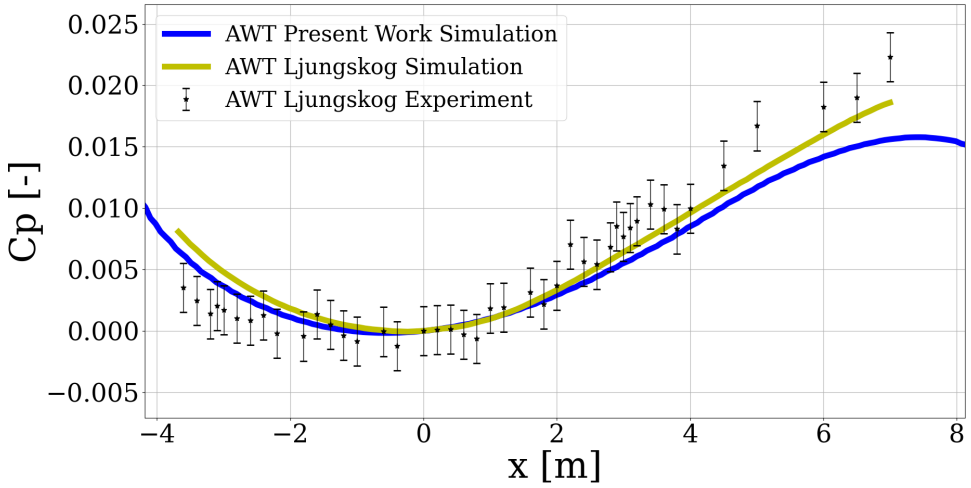

Figure 5.1: Longitudinal pressure gradient in the aerodynamic wind tunnel. Validation against Ljungskog [3]. Note that all the data has been offset so that $C_p(x = 0) = 0$ where $x = 0$ is the center of the car.

The trend of the static pressure coefficient is consistent with both Ljungskog's simulation and experiment. This is an indication that the method developed in this thesis is a good starting point also for the simulations of the other tunnels.

5.2 Aerodynamics Evaluation

This section will evaluate the sensitivity of each wind tunnel to the boundary interference effects presented in Chapter 3.1 by comparing them to open road driving. Then it will be related to the forces like drag and skin friction on the vehicle in the tunnels.

5.2.1 Pressure Gradient and Horizontal Buoyancy

The longitudinal pressure gradient in the empty tunnels is an indicator of the altered drag measurement because the presence of the gradient itself causes horizontal buoyancy. A favorable pressure gradient means that the pressure coefficient drops in the streamwise direction of the flow. Therefore, there is a higher pressure in front of the car and a lower pressure in the rear, resulting in an increased measured drag. Meanwhile, an adverse pressure gradient will decrease it. Figure 5.2 shows the pressure coefficients of the three empty tunnels where $x = 0$ is the coordinate of the center of the car. In the AWT,

the pressure gradient curve is flat at the position of the car, so the influence of horizontal buoyancy on drag is small. Meanwhile, as expected, the two open jet wind tunnels suffer from steeper gradients, with CWT1 being the most affected and CWT2 being moderately affected.

The pressure coefficient is calculated as follows:

$$C_p(x) = \frac{P_s(x) - P_{s,c}}{\frac{1}{2}\rho U_c} \tag{5.1}$$

where P_s is the static pressure, $P_{s,c}$ and U_c are the static pressure and the velocity in the calibration point of a wind tunnel, respectively.

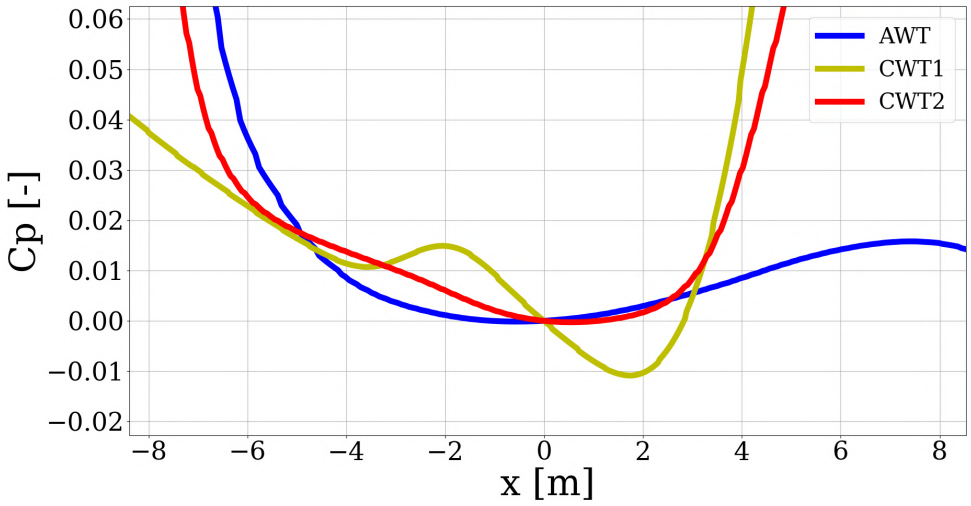

Figure 5.2: Longitudinal pressure gradients in the three wind tunnels. The center of the car is located at $x = 0$. Note that all data has been offset so that $C_p(x = 0) = 0$.

5.2.2 Blockage effects

Nozzle and solid blockage effects in the wind tunnels are qualitatively visualized by means of velocity magnitude around the car in Figure 5.3 compared to open road. As expected, the AWT is the most similar to open road thanks to its wider nozzle and test section and slotted walls that allow the flow to expand in the plenum. However the overall flow velocity is slightly higher, mainly due to the flow acceleration in the nozzle, so a drag deficit is expected. The two climatic wind tunnels with open jet layout are more sensitive to blockage effects. The CWT1, with its small nozzle and the car being positioned very close to it, has a significant flow acceleration in the

nozzle and wide jet expansion. It results in high velocity in the front of the car and around the front wheels and substantial deceleration in the rear due to over-expansion. The CWT2 follows similar patterns seen for the CWT1 due to the same open jet layout, however its wider nozzle and the increased car distance from it show minimal jet expansion and a moderate velocity variation when compared to open road driving. The blockage effects in the two CWTs cause a lower drag on the front that will be excessively recovered in the rear.

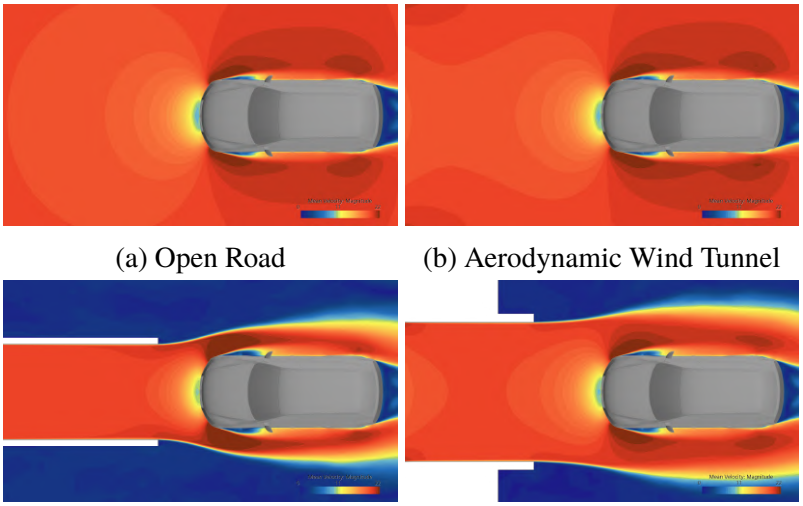

(a) Open Road (b) Aerodynamic Wind Tunnel

(c) Old Climatic Wind Tunnel (d) New Climatic Wind Tunnel

Figure 5.3: Velocity magnitude around the vehicle in open road and wind tunnels. Contour plots to visualize the blockage effects.

The flow acceleration around the front of the car is plotted in Figure 5.4 where the white dotted probe line is where the x-component of the velocity is measured.

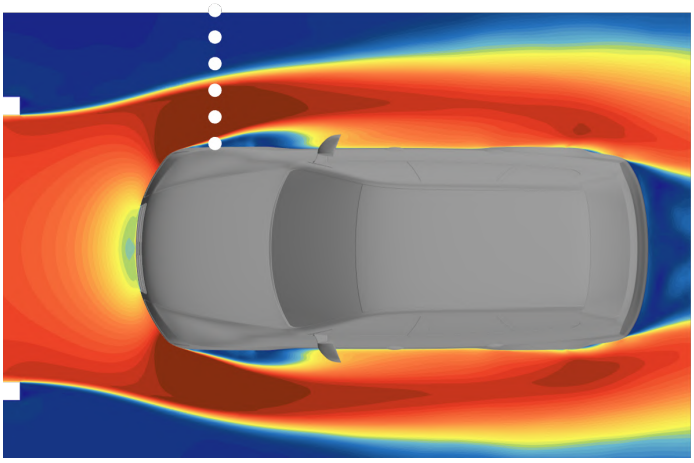

(a) White dotted probe line for x-component of velocity

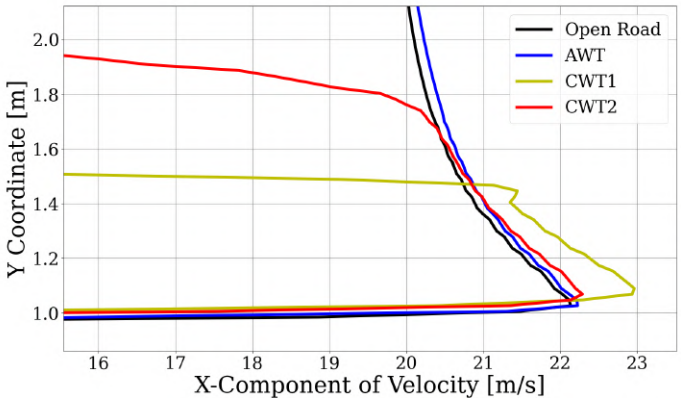

(b) Plot of x-component of velocity

Figure 5.4: X-Component of velocity measured on the side of the vehicle for open road and wind tunnels at height $z = 0.7$m. $y = 0$ is the centerline of the car.

5.2.3 Aerodynamic Forces

Different flow fields in the wind tunnels imply different force distributions on the test vehicle. In this section the drag and skin friction coefficient will be evaluated.

5.2.3.1 Drag Force

As described in the previous section, the flow field in the AWT does not deviate significantly from the open road scenario; thus, the gap in the measured drag is minimal. Meanwhile, the blockage effects in the two CWTs cause a non-

negligible flow acceleration in the nozzle and over-expansion around the car. This leads to earlier flow separation at the front with lower front drag. Figure 5.5 illustrates this phenomenon. The drag is then recovered at the rear due to a lower pressure wake and velocity drop as depicted in Figure 5.6. The comprehensive understanding of the development of the drag force on the car is provided by the cumulative drag plot in Figure 5.7 that compares the wind tunnels and open road.

Although the local drag distribution in the CWT2 is not ideal due to its prominent divergence from open road, the total drag prediction is actually better than anticipated.

It is not possible to say the same for the CWT1 which is too sensitive to blockage effects. The local drag deficit and total drag prediction are too inaccurate to suggest this tunnel for any aerodynamic testing.

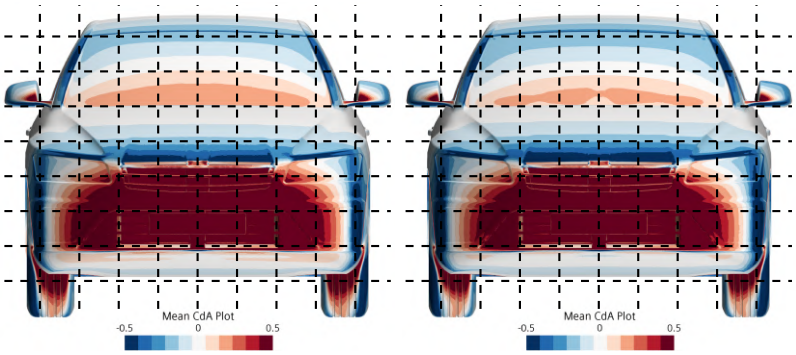

(a) Open Road (b) Aerodynamic Wind Tunnel

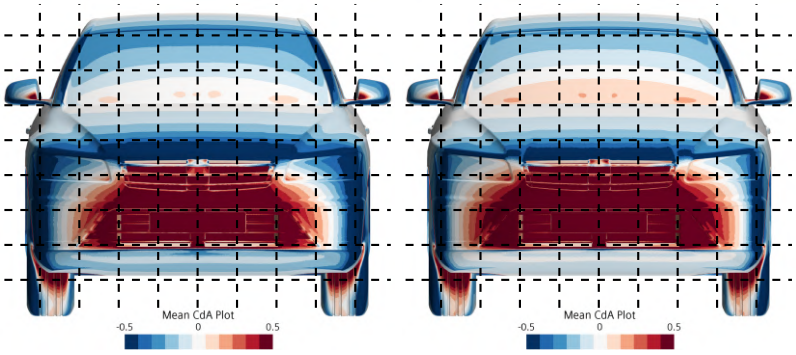

(c) Old Climatic Wind Tunnel (d) New Climatic Wind Tunnel

Figure 5.5: Comparison of front drag distribution on the vehicle surface in the wind tunnels and open road.

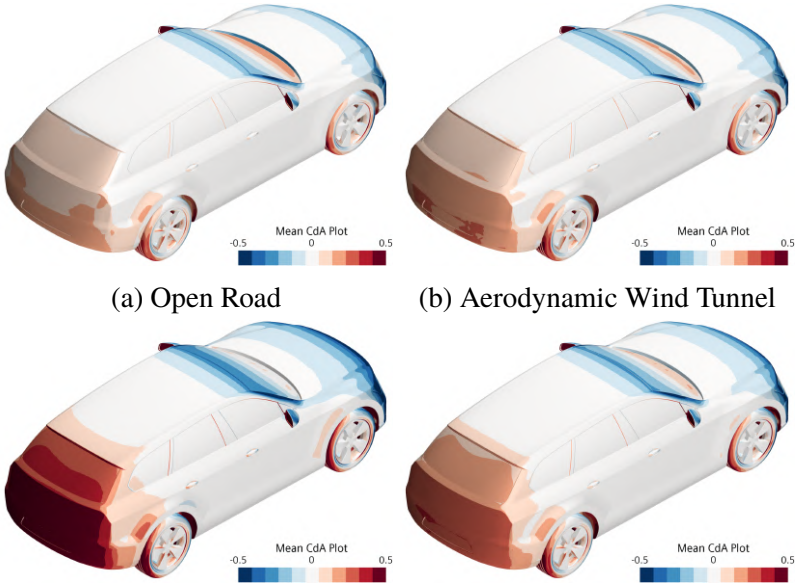

(a) Open Road (b) Aerodynamic Wind Tunnel

(c) Old Climatic Wind Tunnel (d) New Climatic Wind Tunnel

Figure 5.6: Comparison of rear drag distribution on the vehicle surface in the wind tunnels and open road.

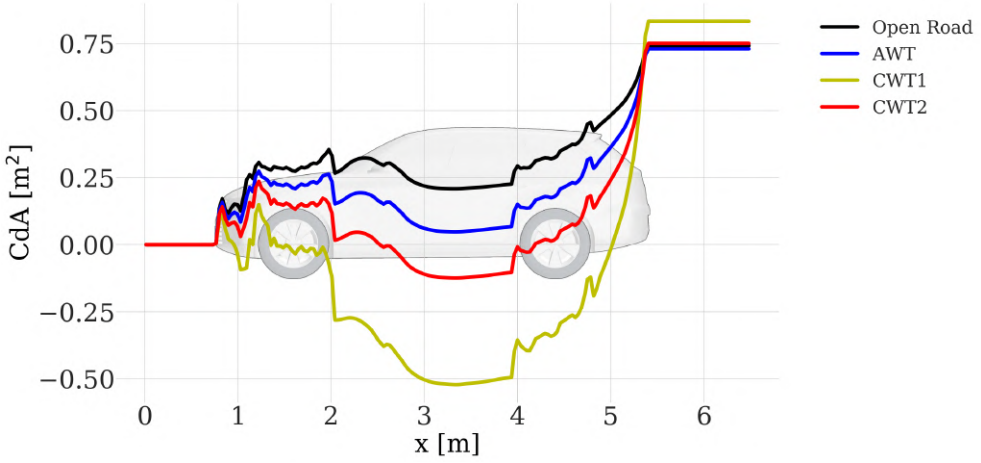

Figure 5.7: Cumulative drag plot of the vehicle in the wind tunnels and open road

5.2.3.2 Skin Friction Coefficient

The skin friction coefficient is a pertinent quantity to evaluate in contamination tests because it is responsible for wall-bounded water transport and it can alter the soiling patterns on the vehicle.

Despite setting the stick boundary condition for droplet impact on walls, measuring and comparing the skin friction coefficient is pertinent to assess the reliability of the soiling results.

The areas investigated are shown in Figure 5.8 and the percentage variations of the relative skin friction coefficient with respect to open road values in Figure 5.9. It is good practice to establish an arbitrary threshold under which the variations are not considered relevant. For this work it was chosen to set it to 5%.

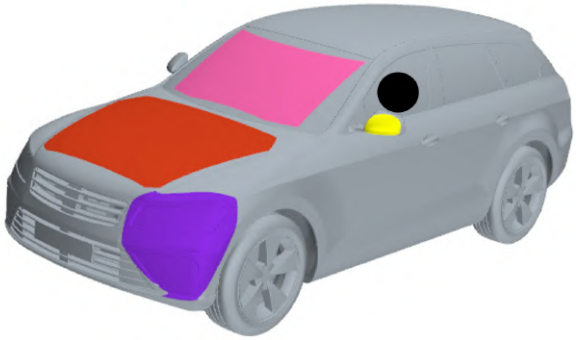

Figure 5.8: Areas of measurement for skin friction coefficient.

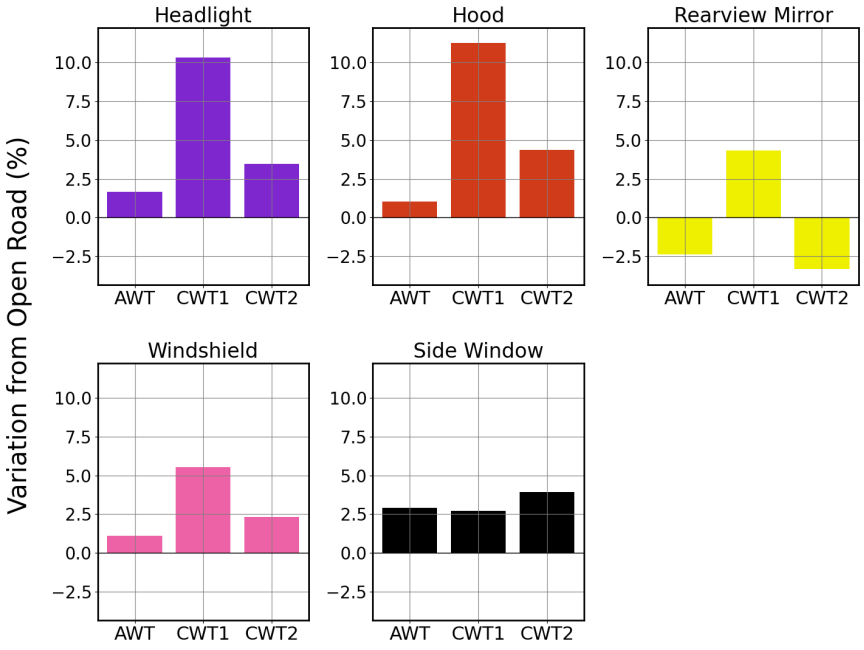

Figure 5.9: Bar plot for skin friction coefficient in the three wind tunnels normalized by open road values.

Once again, the AWT is the tunnel that has the least variation from open road, followed by the CWT2. Both always remain below the stated threshold. On the other hand, CWT1 definitely has greater skin friction with some variations beyond 10%.

5.3 Contamination

In this section, the contamination of the car in the wind tunnels is evaluated. The results are presented in order of particle size: 5 µm, 50 µm, 200 µm. For each of them, the soiling areas on the car are visually inspected and then a plot of the accumulated rain mass normalized by the open road values is illustrated.

5.3.1 Small Droplets - 5 µm

The small droplets have an extremely short relaxation time, which means that they immediately adjust to most perturbations in the flow field. This results in the droplets also following small-scale eddies such as in the boundary layer, therefore sticking all over the car in all the wind tunnels as indicated in Figures 5.10 and 5.11.

The difference is the amount of rain impacts: the cars in the AWT and the CWT2 collect roughly the same water as the one in the open road, while the car in the CWT1 gets almost twice that amount as shown in Figure 5.12. This is due to the overall higher vorticity and the proximity of the shear layers to the vehicle in the CWT1 due to its small nozzle size. This phenomenon transports more droplets all over the car.

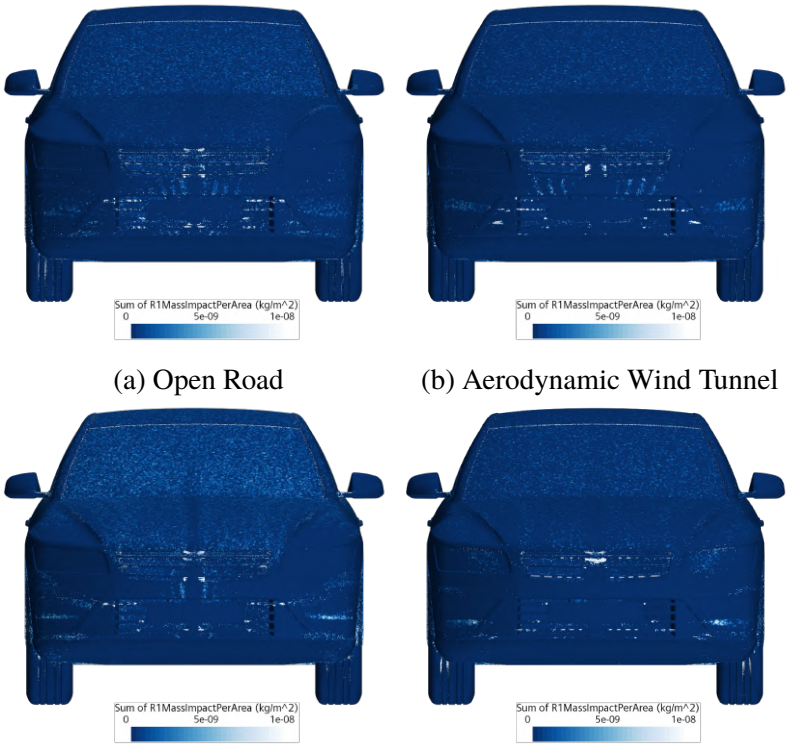

(a) Open Road (b) Aerodynamic Wind Tunnel

(c) Old Climatic Wind Tunnel (d) New Climatic Wind Tunnel

Figure 5.10: Comparison of small droplets impact areas on the front of the car in the wind tunnels and open road.

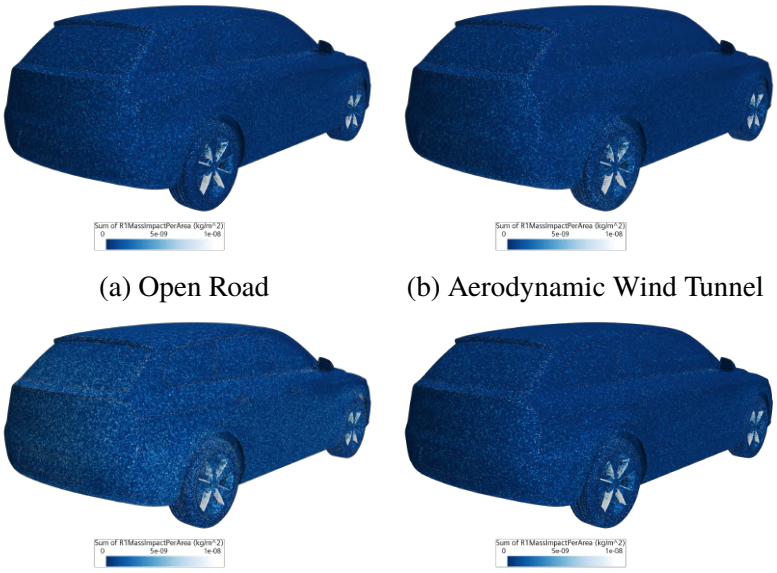

(a) Open Road (b) Aerodynamic Wind Tunnel

(c) Old Climatic Wind Tunnel (d) New Climatic Wind Tunnel

Figure 5.11: Comparison of small droplets impact areas on the rear and side of the car in the wind tunnels and open road.

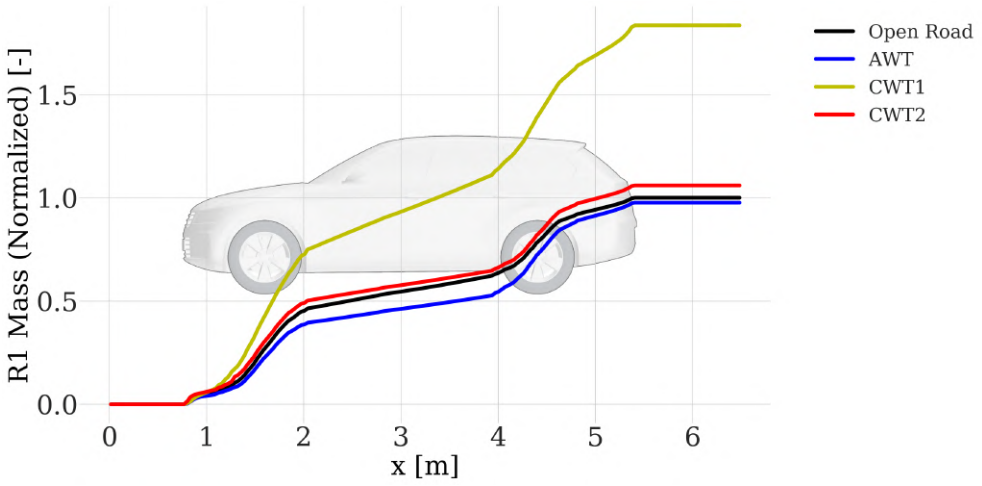

Figure 5.12: Accumulated small rain droplets on the car in the wind tunnels and open road.

5.3.2 Medium Droplets - 50 µm

The 50 µm droplets, due to their higher inertia, are less influenced by the airflow. They tend to impact the front grille due to their momentum. The

soiling pattern visible in Figure 5.13 is consistent between the three wind tunnels. However, they all differ in the same way from the open road scenario where the impact areas are more scattered on the front grille and license plate due to the more gradual velocity gradient of the flow approaching the car. The steeper gradient in the wind tunnels is due to the nozzle blockage effect shown in Figure 5.3.

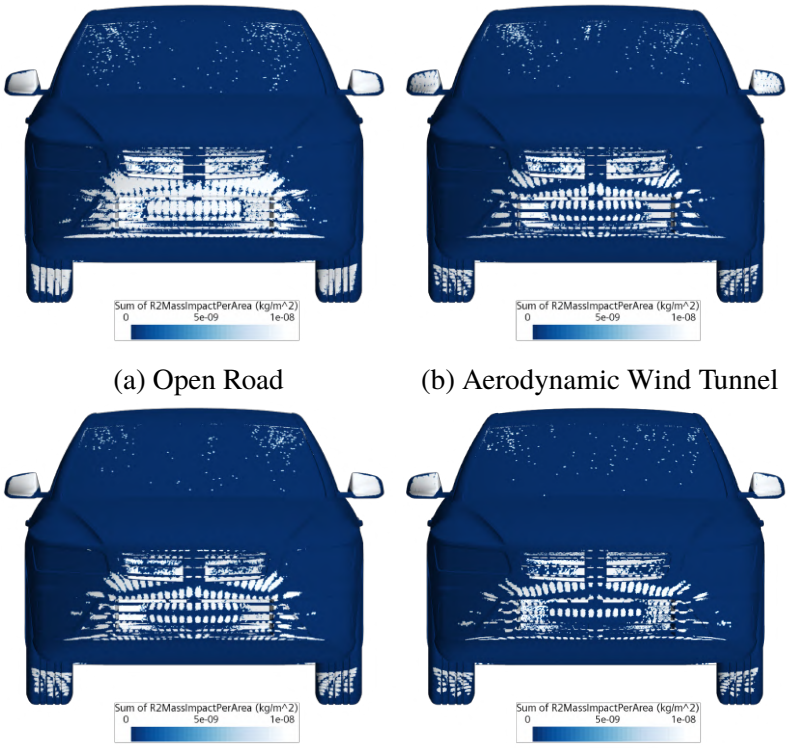

(a) Open Road (b) Aerodynamic Wind Tunnel

(c) Old Climatic Wind Tunnel (d) New Climatic Wind Tunnel

Figure 5.13: Comparison of medium droplets impact areas on the front of the car in the wind tunnels and open road.

Once the flow separates from the surface of the car, the droplets will not impact it until the flow reattaches on the sides. Furthermore, these droplets recirculate in the turbulent wake of the vehicle and cause substantial soiling in the rear, as in Figure 5.14. The sides and rear contamination in all simulations is nearly identical, just as the total rain mass accumulated on the car is similar as shown in the cumulative plot in Figure 5.15. However, the car in the CWT1 generally collects more rain and is also wet on the roof due to the shear layer droplet transport.

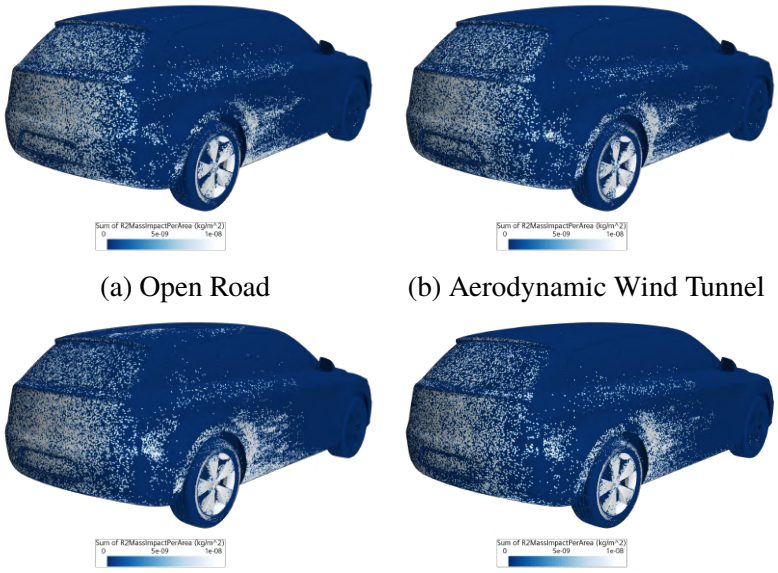

(a) Open Road (b) Aerodynamic Wind Tunnel

(c) Old Climatic Wind Tunnel (d) New Climatic Wind Tunnel

Figure 5.14: Comparison of medium droplets impact areas on the rear and side of the car in the wind tunnels and open road.

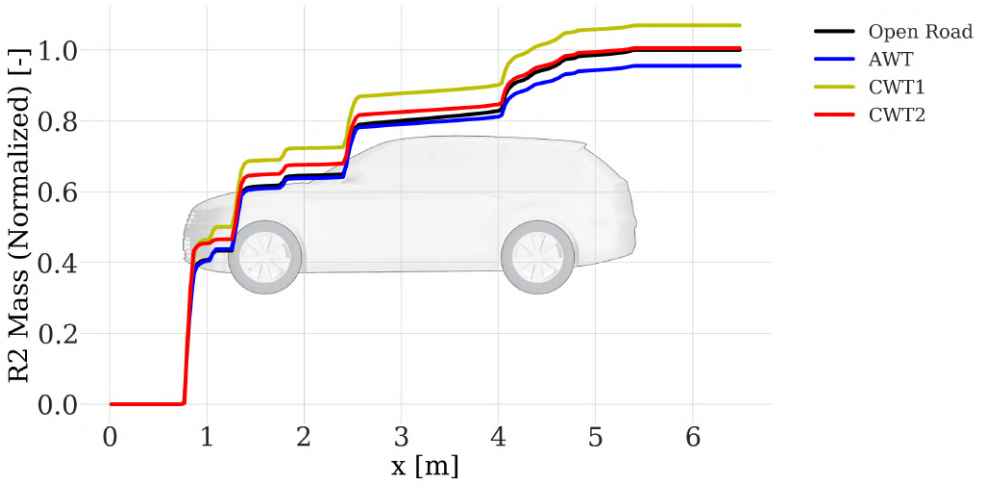

Figure 5.15: Accumulated medium rain droplets on the car in the wind tunnels and open road.

5.3.3 Large Droplets - 200 µm

The 200 µm droplets are the largest simulated. Due to their inertia, they impact the front of the car in the same way as they require an extremely high response

time to follow the sudden flow deviations. See Figure 5.16.

There is barely any soiling on the sides, roof and rear of the vehicle in open road, AWT and CWT2 due to the droplets not being sensitive to the airflow. Only for the car in the CWT1 there is significant rain deposit on the roof and sides, as illustrated by Figures 5.17 and 5.18. Again, this is attributed to the high vorticity level in proximity of the car induced by the shear layers that manage to influence the trajectories of such particles.

The total rain mass collected on the cars is basically the same in all the wind tunnels and open road as shown in 5.19. Still, this plot does not capture the larger amount of rain deposited on the sides and roof in the CWT1. The reason is that such increase is almost negligible compared to the rain deposited on the front. Therefore, the plot for the accumulated rain mass in the rear is provided in Figure 5.20 in which the measurement starts at a further X coordinate.

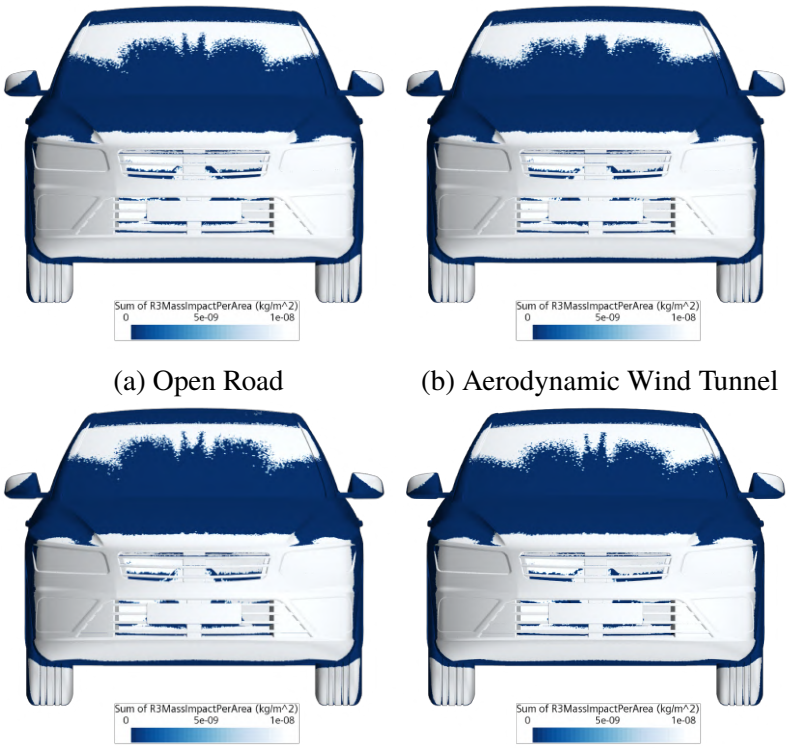

(a) Open Road (b) Aerodynamic Wind Tunnel

(c) Old Climatic Wind Tunnel (d) New Climatic Wind Tunnel

Figure 5.16: Comparison of large droplets impact areas on the front of the car in the wind tunnels and open road.

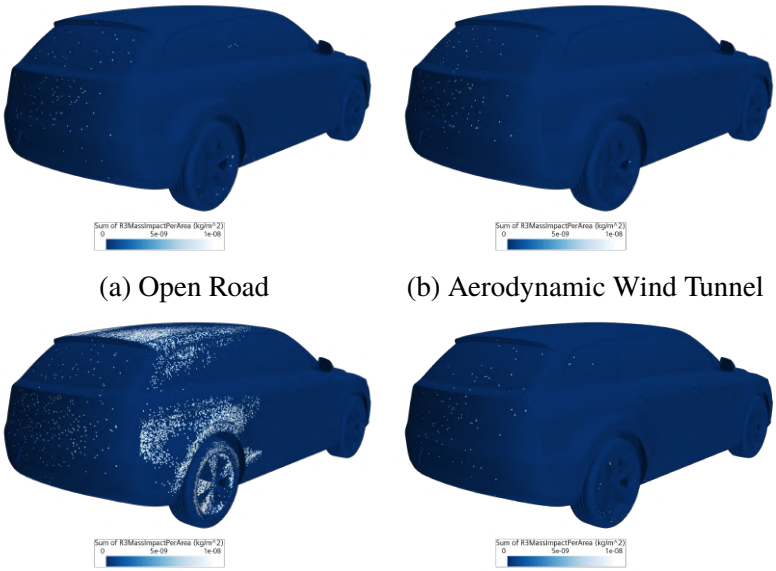

(a) Open Road (b) Aerodynamic Wind Tunnel

(c) Old Climatic Wind Tunnel (d) New Climatic Wind Tunnel

Figure 5.17: Comparison of large droplets impact areas on the rear and side of the car in the wind tunnels and open road.

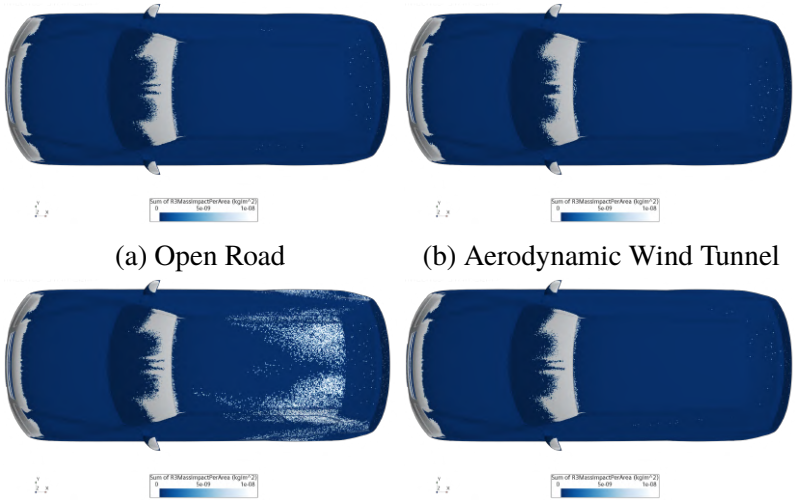

(a) Open Road (b) Aerodynamic Wind Tunnel

(c) Old Climatic Wind Tunnel (d) New Climatic Wind Tunnel

Figure 5.18: Comparison of large droplets impact areas on the roof of the car in the wind tunnels and open road.

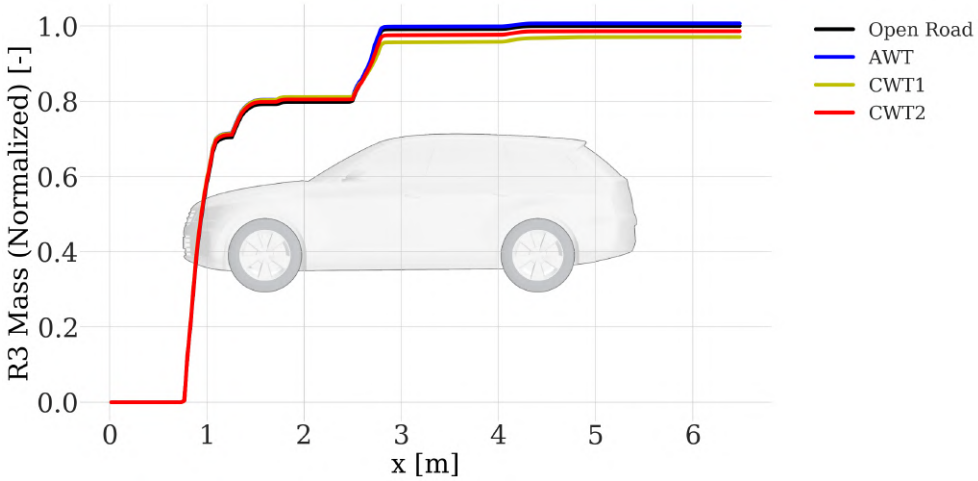

Figure 5.19: Accumulated large rain droplets on the car in the wind tunnels and open road.

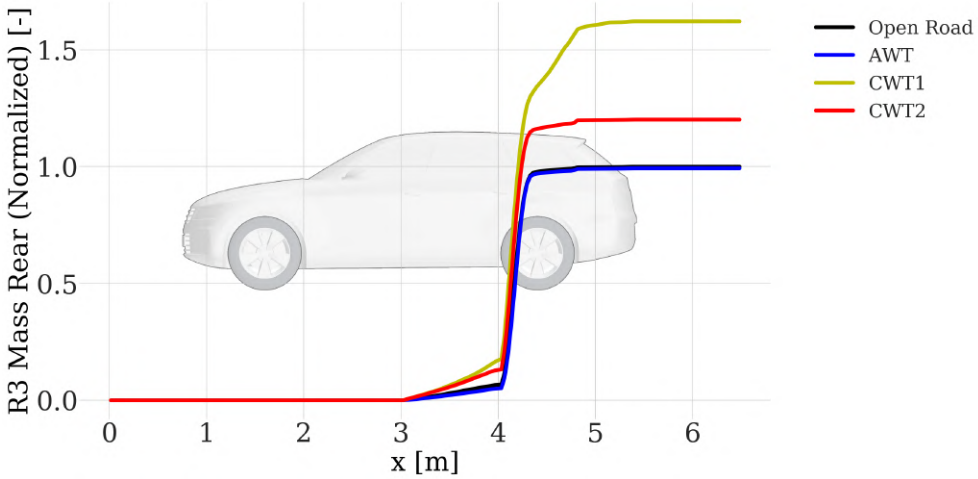

Figure 5.20: Accumulated large rain droplets on the rear of the car in the wind tunnels and open road.

5.4 Turbulence Generator

In this section the influence of a turbulence generator in the CWT2 is investigated from a contamination perspective and will be compared with the CWT2 baseline. The turbulence generator is made up of four horizontal bars. Its geometry and positioning in the CWT2 is shown in Figure 5.21. The skin friction coefficient, impact areas and total rain mass will be evaluated.

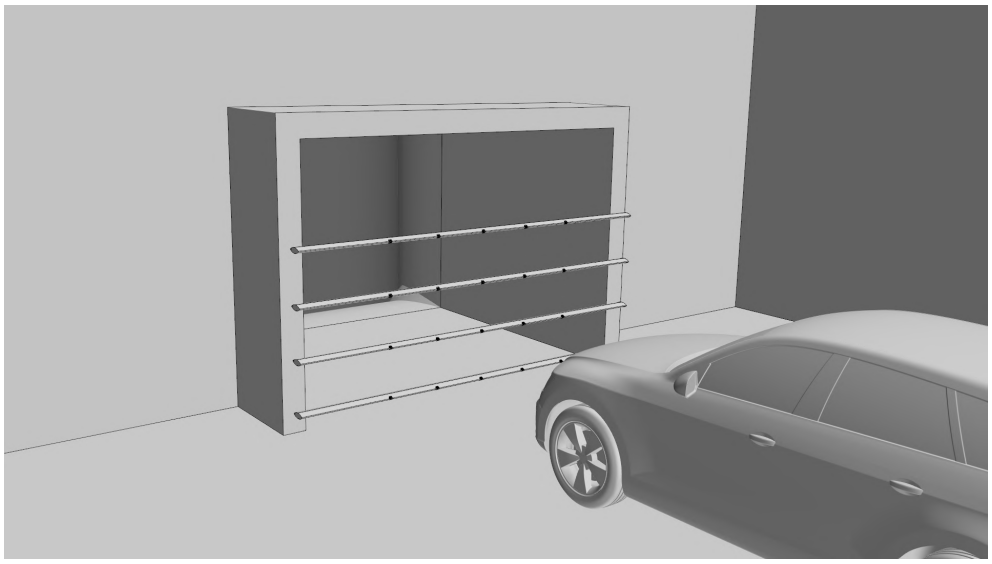

Figure 5.21: Turbulence generator in the new climatic wind tunnel.

5.4.1 Skin Friction Coefficient

There is a general increase in skin friction coefficient when using the turbulence generator. However, its effects are very localized in the wake of its four horizontal bars and that is the reason for the extreme increase for the rearview mirror as presented in the bar plot in Figure 5.22.

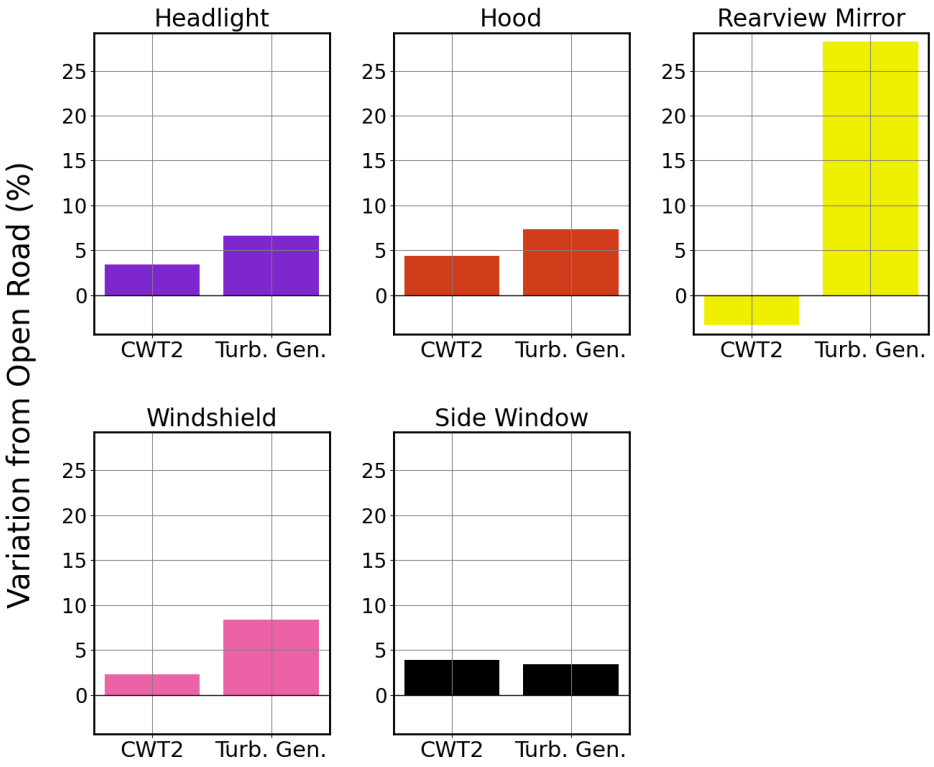

Figure 5.22: Bar plot for skin friction coefficient in the new climatic wind tunnel with and without turbulence generator normalized by open road values.

5.4.2 Small Droplets - 5 µm

Consistently with what has previously been described, an increase in the turbulence level of the flow results in more rain impacts on the car for the small droplets all over the car as illustrated in Figures 5.23 and 5.24. Moreover, according to the cumulative plot of the rain mass in Figure 5.25, the deposit of small droplets almost triples when using this turbulence generator.

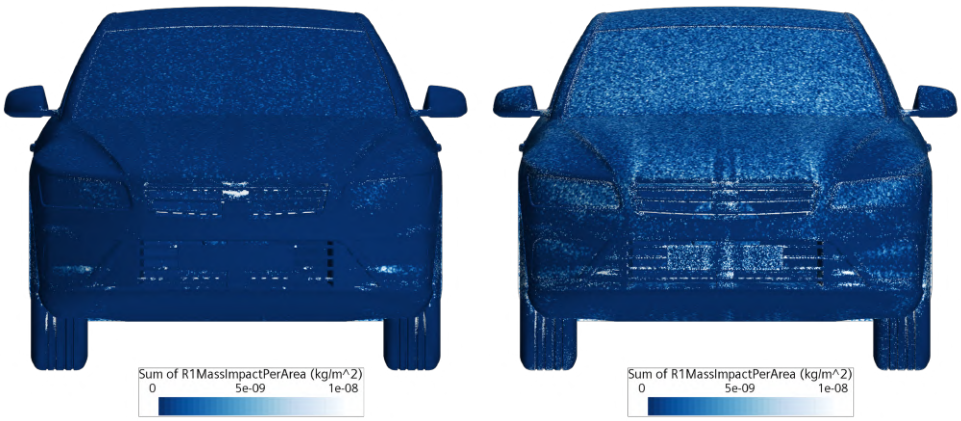

(a) CWT2 without turbulence generator (b) CWT2 with turbulence generator

Figure 5.23: Comparison of small droplets impact areas on the front of the car in the new climatic wind tunnel with and without turbulence generator.

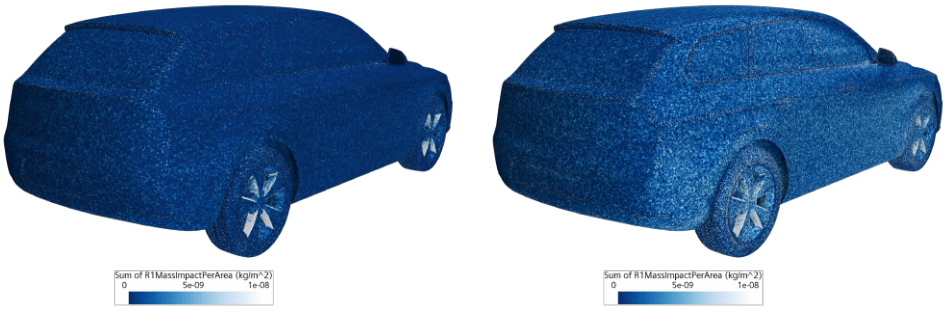

(a) CWT2 without turbulence generator (b) CWT2 with turbulence generator

Figure 5.24: Comparison of small droplets impact areas on the rear and side of the car in the new climatic wind tunnel with and without turbulence generator.

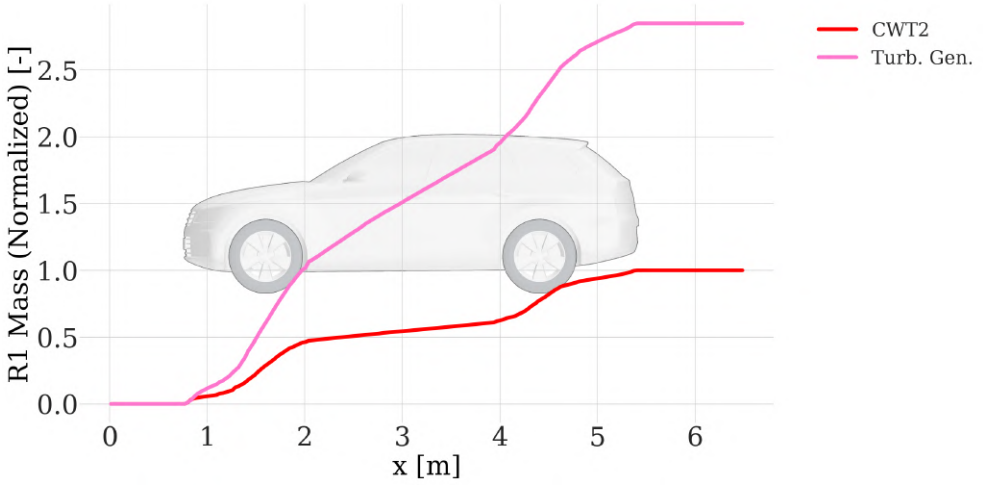

Figure 5.25: Accumulated small rain droplets on the car in the new climatic wind tunnel with and without turbulence generator.

5.4.3 Medium Droplets - 50 µm

The use of the turbulence generator also leads to a higher accumulation of medium rain droplets. However, in this case the increment in rain deposit is minimal as shown in Figure 5.28. The most interesting difference lies in the front contamination portrayed by Figure 5.26 where the localized vorticity induced in the wake of the turbulent generator affects the front grille and windshield. The rain impacts on the front grill are more chaotic and distributed and the windshield is now completely covered in rain.

(a) CWT2 without turbulence generator (b) CWT2 with turbulence generator

Figure 5.26: Comparison of medium droplets impact areas on the front of the car in the new climatic wind tunnel with and without turbulence generator.

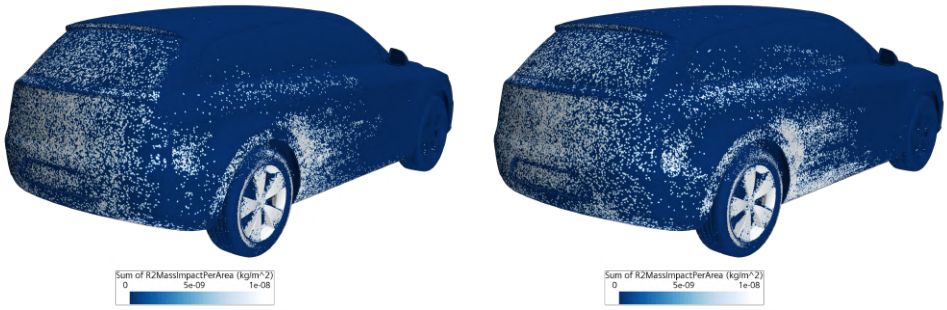

(a) CWT2 without turbulence generator (b) CWT2 with turbulence generator

Figure 5.27: Comparison of medium droplets impact areas on the rear and side of the car in the new climatic wind tunnel with and without turbulence generator.

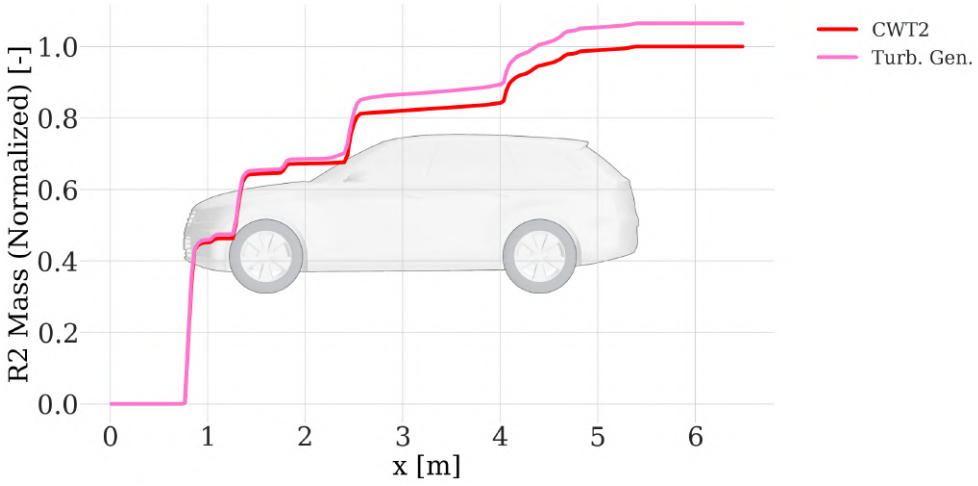

Figure 5.28: Accumulated medium rain droplets on the car in the new climatic wind tunnel with and without turbulence generator.

5.4.4 Large Droplets - 200 µm

The effect of the turbulent generator on the distribution of large rain droplets on the windshield is consistent with what has been shown for the medium ones. In fact, the area of the windshield affected by water is wider than it would be without the turbulence generator according to Figure 5.29. However, there is an inverted trend for these particles which results in a lower amount of rain mass impacting the vehicle as shown in Figure 5.31.

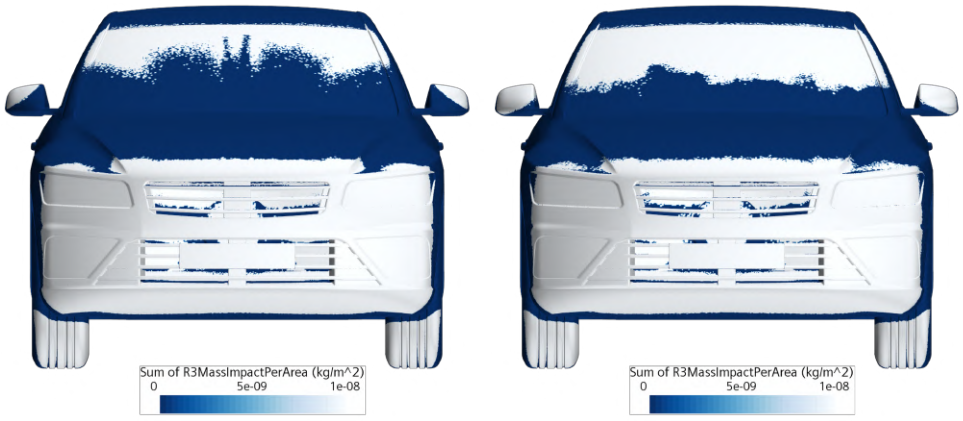

(a) CWT2 without turbulence generator (b) CWT2 with turbulence generator

Figure 5.29: Comparison of large droplets impact areas on the front of the car in the new climatic wind tunnel with and without turbulence generator.

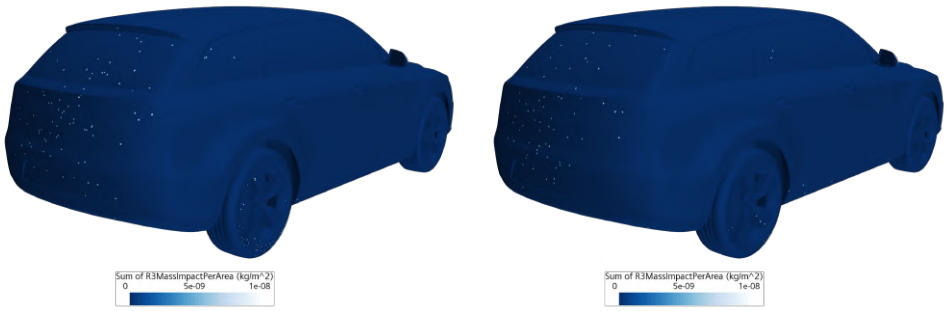

(a) CWT2 without turbulence generator (b) CWT2 with turbulence generator

Figure 5.30: Comparison of large droplets impact areas on the rear and side of the car in the new climatic wind tunnel with and without turbulence generator.

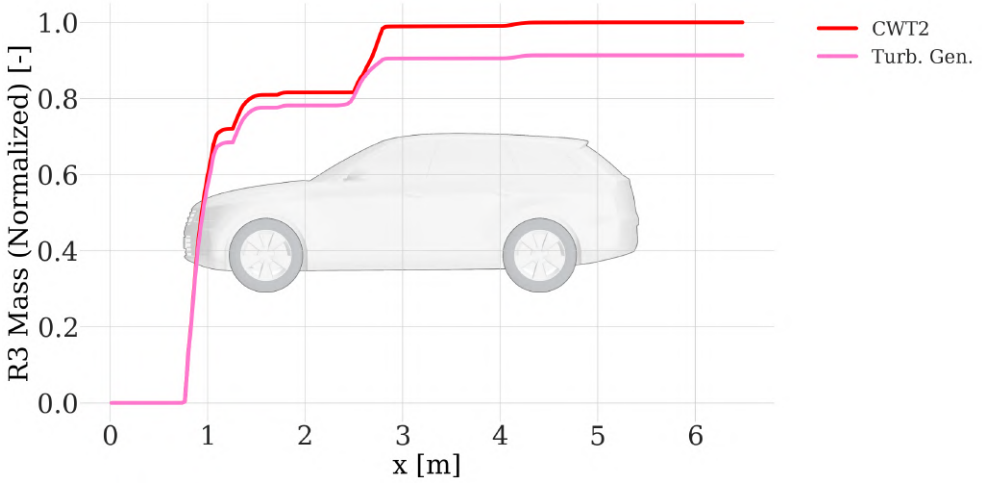

Figure 5.31: Accumulated large rain droplets on the car in the new climatic wind tunnel with and without turbulence generator.

Chapter 6

Conclusions

This thesis focused on the evaluation of aerodynamic performance and particle dynamics in three different wind tunnels at Volvo Cars. Through CFD simulations, the unique characteristics of each wind tunnel were analyzed to understand their suitability for specific applications. The findings provide valuable insights on the design features and layouts of wind tunnels for automotive testing, highlighting the importance of considering boundary interference effects and their impact on aerodynamic and contamination testing. An open road simulation has been setup as benchmark to evaluate the three wind tunnels. However, it is important to keep in mind that the real life scenario of a customer is an open empty road without disturbances. Such open road scenario aims to represent an ideal wind tunnel that does not experience any kind of boundary interference.

6.1 Aerodynamic Wind Tunnel

The Aerodynamic Wind Tunnel (AWT) has demonstrated exceptional accuracy in predicting the aerodynamic field around the car and its drag force distribution. The close resemblance of its airflow with open road conditions makes it a reliable tool for contamination testing. The skin friction coefficient shows negligible variations from open road values, which, along with comparable soiling patterns, is expected to guarantee comparable rain deposit and even wall-bounded water transport phenomena. Overall, the AWT provides highly accurate aerodynamic and contamination results, making it a valuable facility for automotive testing.

6.2 Old Climatic Wind Tunnel

The Old Climatic Wind Tunnel (CWT1) exhibits significant inaccuracies when compared to open road simulations. The small nozzle and close proximity of the car to it result in high boundary interference, causing flow over-expansion and an extremely low-pressure wake. These factors lead to inaccurate force predictions and higher skin friction. The increased vorticity and shear layers result in more contamination, making CWT1 unsuitable for predicting open road soiling. However, it may be more comparable to third-party contamination scenarios, such as driving behind a truck.

6.3 New Climatic Wind Tunnel

The New Climatic Wind Tunnel (CWT2) generally replicates open road conditions quite well. It provides a good overall airflow and total drag prediction, although it suffers from blockage effects that alter local drag distribution. The skin friction coefficient variations from open road values are within the chosen 5% variation threshold, ensuring realistic contamination patterns. The CWT2 competes with the AWT in rain contamination testing, which sometimes shows minimal difference depending on the droplet size. Future snow tests in CWT2 would be interesting since they are not possible in the AWT.

6.4 Turbulence Generator

The turbulence generator used in the new climatic wind tunnel is composed of four horizontal bars. It causes localized vorticity in the wake of the bars that locally alter the airflow and particle transport. Although it provided useful insights in artificially inducing turbulence in a wind tunnel, the desired outcome was to achieve widespread vorticity throughout the entire test section.

Chapter 7

Future work

Given the broad applicability of this research subject, there are several areas where further analysis and exploration can enhance the accuracy and applicability of wind tunnel simulations. This section lists outlines key areas for possible future work, focusing on improving simulation fidelity, generalizing the applicability of the findings and addressing limitations of this study.

- **Implementation of flow conditioning devices:** one key area to improve accuracy and applicability of wind tunnels simulations is the modeling and implementation of flow conditioning devices which has not been taken into account in this thesis. For instance suction systems, tangential blowers, wheel drive units, belts and moving floors significantly improve the airflow compared to open road conditions.

- **Optimization of droplet injection point:** another important aspect to consider is improving the injectors grid which may not be optimal for all wind tunnels and not realistically represent open road conditions. This could help the development of ad-hoc solutions for rain injection devices for each wind tunnel.

- **Wheel injectors for self-contamination:** this thesis focused only on external (or third party) contamination. However, driving on a wet road causes water droplets to be lifted by the wheels of the car and contaminate itself. The modeling and implementation of wheel injection points can expand the current state of this work.

- **Simulation of different particle sizes:** the droplet sizes chosen for this work represent a wide range of rain scenarios. Nevertheless, it would

be appropriate to conduct particle measurement studies for different rain conditions followed by an exterior soiling investigation for those.

- **Snow testing:** contamination is a wide research area. Expanding this work to snow testing would be useful for regions with colder climates that experience different kinds of adverse weather conditions and understand the safety implications of snow on driver visibility and sensor obstruction.
- **Testing of different velocities:** even though in adverse driving conditions lower speeds are expected, it would still be useful to investigate the applicability of wind tunnels for exterior soiling at higher speeds. Furthermore, the sensitivity of wind tunnels to boundary interference effects might vary.
- **Considering more boundary interference effects:** in this thesis only blockage and horizontal buoyancy have been discussed. A further step can be the evaluation of other effects such as wake-induced, collector and diffuser effects.
- **Correction methods:** applying correction methods for boundary interference effects can help understanding which ones alter the measurement the most in each wind tunnel. This is relevant mainly for understanding the aerodynamic properties of the tunnels, rather than the contamination aspect.
- **Different car positioning:** testing different car positions in the tunnels could help improve the contamination patterns.

References

[1] D. Eisenberg and K. Warner, "Effects of snowfalls on motor vehicle collisions, injuries, and fatalities," *American journal of public health*, vol. 95, pp. 120–4, 02 2005. doi: 10.2105/AJPH.2004.048926 [Page 1.]

[2] T. Eidevåg, "Snow contamination of cars: Adhesive particle collisions with exterior surfaces," Ph.D. dissertation. ISBN 9789179056667 2022. [Online]. Available: https://research.chalmers.se/publication/530277 [Page 1.]

[3] E. Ljungskog, "Evaluation and modeling of the flow in a slotted wall wind tunnel," Ph.D. dissertation, 2019. [Online]. Available: https://research.chalmers.se/publication/514006 [Pages ix, xiii, 5, 13, 15, 16, 17, 27, and 28.]

[4] Y. Zhang, J. Li, Z. Zhang, W. Yuan, J. Zhou, C. Shen, and C. Zhang, "Assessment and improvement of rainfall environment reproduction for climatic wind tunnel," *Engineering Applications of Computational Fluid Mechanics*, vol. 18, no. 1, p. 2399671, Dec. 2024. doi: 10.1080/19942060.2024.2399671. [Online]. Available: https://www.tandfonline.com/doi/full/10.1080/19942060.2024.2399671 [Page 5.]

[5] P. K. Kundu, I. M. Cohen, D. R. Dowling, and J. Capecelatro, *Fluid mechanics*. Elsevier, 2024. ISBN 978-0-12-819807-0. [Online]. Available: https://doi.org/10.1016/C2018-0-02033-2 [Page 6.]

[6] A. N. Kolmogorov, "The local structure of turbulence in incompressible viscous fluid for very large reynolds," *Numbers. In Dokl. Akad. Nauk SSSR*, vol. 30, p. 301, 1941. [Page 6.]

[7] J. H. Ferziger, M. Perić, and R. L. Street, *Computational methods for fluid dynamics*. springer, 2019. [Online]. Available: https://link.springer.com/book/10.1007/978-3-642-56026-2 [Page 6.]

[8] R. Courant, K. Friedrichs, and H. Lewy, "On the partial difference equations of mathematical physics," *IBM Journal of Research and Development*, vol. 11, no. 2, pp. 215–234, 1967. doi: 10.1147/rd.112.0215. [Online]. Available: https://ieeexplore.ieee.org/abstract/document/5391985/ [Page 7.]

[9] J. Smagorinsky, "General circulation experiments with the primitive equations: I. the basic experiment," *Monthly Weather Review*, vol. 91, no. 3, pp. 99–164, 1963. [Page 8.]

[10] S. B. Pope, *Turbulent flows*, 1st ed. Cambridge: Cambridge Unive. Press, 2000. ISBN 978-0-521-59886-6 [Page 8.]

[11] P. Spalart, W.-H. Jou, M. Strelets, and S. Allmaras, "Comments on the feasibility of les for wings, and on a hybrid rans/les approach," 1997. [Online]. Available: https://www.researchgate.net/publication/236888805 [Page 8.]

[12] V. L. Schiller, "Uber die grundlegenden berechnungen bei der schwerkraftaufbereitung," *Z. Vereines Deutscher Inge.*, vol. 77, pp. 318–321, 1933. [Page 10.]

[13] M. Sommerfeld *et al.*, "Theoretical and experimental modelling of particulate flows," *Lecture series*, vol. 6, pp. 3–7, 2000. [Page 11.]

[14] O. Hamidi, "Water contamination of a side view camera monitoring system. understanding how driving conditions and design features affect dynamics of airborne droplets using cfd and experiments," Master's thesis, Chalmers Tekniska Högskola, 2023. [Online]. Available: https://odr.chalmers.se/items/77723780-733c-4dd4-b43d-a141b6fad25c [Page 11.]

[15] K. Cooper, "Bluff-body blockage corrections in closed-and open-test-section wind tunnels," *AGARD, AG-336, NTIS, Springfield, VA*, vol. 6, 1998. [Page 13.]

[16] E. Mercker and J. Wiedemann, "On the Correction of Interference Effects in Open Jet Wind Tunnels," Feb. 1996. doi: 10.4271/960671 p. 960671. [Online]. Available: https://www.sae.org/content/960671/ [Page 15.]

[17] G. Wickern, “A Theoretical Approach towards the Self-Correcting Open Jet Wind Tunnel,” Apr. 2014. doi: 10.4271/2014-01-0579 pp. 2014–01–0579. [Online]. Available: https://www.sae.org/content/2014-01-0579/ [Page 15.]

[18] J. Sternéus, T. Walker, and T. Bender, “Upgrade of the Volvo Cars Aerodynamic Wind Tunnel,” Apr. 2007. doi: 10.4271/2007-01-1043 pp. 2007–01–1043. [Online]. Available: https://www.sae.org/content/2007-01-1043/ [Page 16.]

[19] European Car Aerodynamic Research Association (ECARA). ECARA.org: AeroSUV. Accessed: 2025-01-30. [Online]. Available: https://www.ecara.org/drivaer-1 [Page 22.]

[20] ——. ECARA.org: Reference Models. Accessed: 2025-01-30. [Online]. Available: https://www.ecara.org/reference-models [Page 22.]

[21] A. Borg and R. Vevang, “On the Prediction of Exterior Contamination with Numerical Simulations,” *Fluid Dynamics Center, Volvo Car Corporation, Gothenburg, Sweden*. [Page 23.]

TRITA – SCI-GRU 2025:036